Decision-directed iterative methods for PAPR reduction in optical wireless OFDM systems

Ali Waqar Azim, Yannis Le Guennec, Ghislaine Maury

Decision-Directed Iterative Methods for PAPR Reduction in Optical Wireless OFDM Systems

Ali W. Azim[a,*], Yannis Le Guennec[a], Ghislaine Maury[a]

[a] *Université Grenoble Alpes; IMEP-LAHC, 3 Parvis Louis Néel, CS 50257, F-38016 Grenoble, France.*

Abstract

In this paper, we propose two iterative decision-directed methods for peak-to-average power ratio (PAPR) reduction in optical-orthogonal frequency division multiplexing (O-OFDM) systems. The proposed methods are applicable to state-of-the-art intensity modulation-direct detection (IM-DD) O-OFDM techniques for optical wireless communication (OWC) systems, including both direct-current (DC) biased O-OFDM (DCO-OFDM), and asymmetrically clipped O-OFDM (ACO-OFDM). Conventional O-OFDM suffers from high power consumption due to high PAPR. Clipping the O-OFDM signal to a predefined threshold is a simple and efficient method to counteract the high PAPR. However, because of clipping, an inevitable distortion occurs due to the loss of useful information, thus, clipping mitigation methods are required. The proposed iterative decision-directed methods operate at the receiver, and recover the lost information by mitigating the clipping distortion. Simulation results acknowledge that the high PAPR of O-OFDM can be significantly reduced using clipping, and the proposed methods can successfully mitigate the degrading effects of clipping with a much lower computational complexity compared to standard PAPR reduction methods.

Keywords: Intensity modulation-direct detection, optical-orthogonal frequency division multiplexing, peak-to-average power ratio, iterative decoding, clipping, clipping distortion, decision-directed.

1. Introduction

Orthogonal frequency division multiplexing (OFDM) is regarded as a promising modulation scheme for modern communication systems, as it offers high data rate, high spectral efficiency, and an inherent resilience to combat inter-symbol-interference (ISI) resulting from multipath propagation. Recently, optical-OFDM (O-OFDM) has been explored as a potential modulation scheme for optical wireless communication (OWC) systems; by the virtue of added benefits like low cost front ends, immunity to fluorescent-light noise near the DC region, large unlicensed optical spectrum, no electromagnetic interference and eye safety constraints like infrared [1–4]. Moreover, with onset

*Corresponding author. Tel./fax: +33-660-380-994

Email addresses: azima@minatec.grenoble-inp.fr (Ali W. Azim), leguennec@minatec.grenoble-inp.fr (Yannis Le Guennec), ghislaine.maury@minatec.grenoble-inp.fr (Ghislaine Maury)

of incoherent high power light emitting diodes (LEDs) and highly sensitive photo-detectors (PDs), OWC systems have gained an increasing interest in the recent past [5].

In OWC systems, O-OFDM can be employed using a simple and low cost intensity modulation-direct detection (IM-DD) technique. In IM-DD, the data carrying intensity waveform (time-domain O-OFDM signal) is modulated onto the brightness of LED and the light intensity is photo-detected at the receiver. OFDM in its original form has a bipolar and complex time-domain signal, therefore, it is not directly compatible with IM-DD [6]. To be compatible with IM-DD, the time-domain O-OFDM signal is constrained to be real and non-negative. Therefore, O-OFDM techniques are tailored for IM-DD implementation, the two main approaches being: direct-current (DC) biased O-OFDM (DCO-OFDM) [1] and asymmetrically-clipped O-OFDM (ACO-OFDM) [7]. In O-OFDM, a real time-domain signal can be assured by imposing Hermitian symmetry condition in the frequency-domain. Furthermore, to ensure a non-negative time-domain signal for DCO-OFDM, a DC bias is added to the bipolar time-domain signal. However, the addition of DC bias renders the system inefficient due to an increased power consumption. In ACO-OFDM, a non-negative time-domain signal can be obtained by modulating only the odd sub-carriers (sacrificing the even ones) to obtain an anti-symmetric signal, for which the negative amplitudes can be clipped without any loss of useful information. In terms of performance, DCO-OFDM is spectrally more efficient than ACO-OFDM, whereas, ACO-OFDM is more power efficient compared to DCO-OFDM for low order constellations at an expense of reduced spectral efficiency [8].

Despite the advantages, high peak-to-average power ratio (PAPR) remains one of the main limiting factors for O-OFDM performance, and makes it more susceptible to non-linear distortions [2]. Furthermore, PAPR behaviour of O-OFDM is critical in the context of IM-DD, since the LEDs have limited linear dynamic range, clipping distortions exacerbate due to clipping of the signal that lies outside the dynamic range of the LED, and ultimately drastically degrade the system performance. Also, the limited bit resolution of digital-to-analog converters (DACs) and analog-to-digital converters (ADCs) also curb O-OFDM performance, since quantization noise is elevated if a signal with a high PAPR is impinged on them [9].

Several PAPR reduction techniques for O-OFDM have been investigated in the literature. PAPR reduction techniques based on signal transformation concepts like pilot-assisted (PA), selected-mapping (SLM) and partial transmit sequence (PTS) have been studied by Popoola *et al.* [2] and Nadal *et al.* [10], respectively. The use of side information in these methods to retrieve original data block results in a hit on effective data rate and an increase in computational complexity. You and Kahn [11] proposed a block coding technique for PAPR reduction in O-OFDM, this technique has been inherited from Radio Frequency (RF)-OFDM and involves block coding between the information bits and the amplitudes that have been modulated onto the sub-carriers. In another approach by Kang and Hranilovic [12], in-band trellis coding and out-of-band carrier design has been introduced to reduce the negative peaks of the electrical signal. The techniques [11, 12], however, require an increased transmission bandwidth. Furthermore, three distinct single-carrier frequency-domain equalization (SCFDE) techniques have been introduced for IM-DD in [13]. Most of the SCFDE techniques are spectrally less efficient as compared to both DCO- and ACO-OFDM,

except ACO-SCFDE which has the same spectral efficiency (related to the number of data-carrying sub-carriers) as ACO-OFDM. Discrete Fourier transform (DFT)-spread technique is considered as an efficient method to reduce the high PAPR of OFDM signals. For IM-DD, DFT-spread based PAPR reduction techniques have been proposed by Zhou *et al.* [14] and Fulai *et al.* [15]. However, Wu *et al.* [16] have pointed out that due to the Hermitian symmetry requirement in IM-DD, DFT-spread O-OFDM still exhibits high PAPR. Similar conclusions have been drawn in [14] and [15], where it has been reported that the reduction in PAPR is not significant if only DFT-spread technique is used for O-OFDM. So, to be more efficient in terms of PAPR reduction, additional PAPR reduction techniques are also needed along with DFT-spread technique. Consequently, in [14], the authors have combined DFT-spread for ACO-OFDM (which we will refer to as DFT-ACO-spread) with amplitude clipping, and in [15], authors combine DFT-spread based modulation for IM-DD with PTS to significantly counteract the high PAPR. Note that, ACO-SCFDE [13] is exactly similar in its implementation to that of DFT-ACO-spread, therefore, in the sequel we will refer to both techniques as ACO-SCFDE. Recently, Discrete Hartley transform (DHT)-spread based ACO-OFDM has been proposed by Zhou and Qiao in [17] and [18]. It has been demonstrated that the DHT-spread techniques exhibit a lower PAPR compared to DFT-spread techniques. However, DHT-spread techniques are only applicable to real constellations e.g., pulse amplitude modulation (PAM), and moreover, with an increase in size of PAM alphabet, the PAPR reduction capability of DHT-spread decreases [17, 18]. DCO- and ACO-OFDM structure specific PAPR reduction methods have also been reported in literature. Zhang *et al.* [19] proposed a PAPR reduction technique for DCO-OFDM based on semi-definite relaxation. Also, a recoverable upper clipping based scheme for ACO-OFDM has been proposed in [20].

Hereby, the high PAPR is counteracted by deliberate clipping of the time-domain O-OFDM signal, thus limiting the signal amplitude to a pre-specified threshold. As clipping degrades the system performance, hence, distortion compensation methods are required to mitigate clipping distortion [21]. It is important to perceive that the clipping characteristics in O-OFDM are distinct from that of RF-OFDM counterparts in following aspects [3]: (i) in RF-OFDM, the time-domain signal is complex-valued, whereas, in O-OFDM, the time-domain signal is constrained to be real; (ii) the main power limitation in O-OFDM is the average optical power rather than average electrical power as in RF-OFDM. Therefore, most of the theory established regarding clipping characteristics for RF-OFDM cannot be directly generalized to O-OFDM. Moreover, we would like to highlight the repercussions of clipping on O-OFDM. In DCO-OFDM, the DC bias required to avoid lower level signal clipping, should be at least equal to the negative peak of the time-domain DCO-OFDM signal, thus, the required average optical power that is directly proportional to the DC bias is high [2, 11]. However, if the DCO-OFDM signal is clipped, in addition to reduction in PAPR, the required DC bias can be significantly lowered, thus, reducing the required average optical power. An analogous concept has been adopted in [22], where the required DC bias has been reduced by clipping the time-domain O-OFDM signal at the transmitter. Furthermore, clipping can also aid in reducing the bits required by the DAC, since, the clipped signal requires less quantization levels, contrary to an un-clipped DCO-OFDM signal [23]. For ACO-OFDM, clipping ensures a reduction of PAPR,

and also reduces the bit resolution requirement of the DAC. Moreover, a thorough investigation on the impact of LED non-linearity (clipping in particular) on O-OFDM has been presented by Dimitrov *et al.* [5], along with analytical models for clipped O-OFDM. Further, [5] also weighs in the impact of clipping on bit-error-rate (BER), power efficiency, etc.

In order to compensate the clipping distortion induced by deliberate clipping of time-domain O-OFDM signal, two receiver-based iterative decision-directed non-linear distortion mitigation methods; Time-Domain Clipped Sample Reconstruction (TDCSR), and Frequency-domain Clipping Distortion Removal (FDCDR), based on Bussgang decomposition in line with [24] and [25], respectively, are proposed for PAPR reduction in O-OFDM systems. Note that, the methods in [24] and [25] cannot be directly used for IM-DD based O-OFDM systems, since they are restricted to be applicable on complex-valued bipolar OFDM signals. Moreover, the methods [24] and [25], are not equipped to handle the DC bias for DCO-OFDM, and the anti-symmetric property of ACO-OFDM. Therefore, the uniqueness of TDCSR and FDCDR comes from the necessity to handle the real-valued nature of time-domain O-OFDM signals, DC bias in DCO-OFDM, anti-symmetric property in ACO-OFDM, and the manner in which the seed for the iterations is updated. The underlying idea of the proposed methods is that if the nonlinear characteristics of the transmitter are known to the receiver, the nonlinear distortions can be perceived as a deterministic function of the received data, and therefore, can be mitigated. TDCSR reconstructs the affected (or lost) clipped samples iteratively in the time-domain, whereas FDCDR estimates the distortion instigated due to clipping and mitigates it iteratively in the frequency-domain. TDCSR and FDCDR are applicable to both DCO- and ACO-OFDM, and are adapted to the constraints imposed by IM-DD. Simulations performed under different clipping conditions show that the proposed methods are capable of significantly mitigating the clipping distortions. Moreover, due to reduction of DC bias, significant reduction in terms of power consumption can be observed for DCO-OFDM. The performance of TDCSR and FDCDR is compared with that of SLM, when clipping mitigation methods are used in conjunction with DCO-OFDM. Since, SCFDE techniques have a low spectral efficiency compared to DCO-OFDM, hence, for a fair comparison, SCFDE techniques have not been used to compare the performance with TDCSR and FDCDR for DCO-OFDM. When ACO-OFDM with clipping mitigation is used, ACO-SCFDE [13] (similar to DFT-ACO-spread) and SLM are used for comparison. It has been noticed that the performance of the proposed methods is superior to that of SLM at a much lower overall complexity for DCO-OFDM. For ACO-OFDM, the performance of the proposed methods is comparable with that of ACO-SCFDE and SLM. Further, clipping can reduce the PAPR to a much lower value, compared to the inherent PAPR reduction capability of ACO-SCFDE and SLM, and also reduces the quantization noise incurred because of the DAC.

1.1. Notation

Unless otherwise mentioned, lower-case boldface letters are used to denote the time-domain vectors e.g., $\boldsymbol{x}$, and lower-case italic letters with an index, e.g., x_n are used to represent the nth element of the time-domain vector, $\boldsymbol{x}$. Discrete Fourier transform (DFT) of time-domain vector is represented by upper case, bold face calligraphic letter, e.g., $\boldsymbol{\mathcal{X}}$. Upper case calligraphic letters with

index, e.g., $\mathcal{X}_k$ denotes the transmitted symbol on kth sub-carrier. Boldface Greek symbols, e.g., $\boldsymbol{\theta}$ are reserved to represent the frequency-domain signals operating within the iterative structure of the proposed methods. Furthermore, we use $E(\cdot)$, $\text{cov}[\cdot]$, $(\cdot)^*$, $|\cdot|$ and $(\cdot)^{\text{T}}$ to represent an ensemble average, covariance, complex conjugate, absolute, and transpose operators, respectively.

1.2. Paper Organization

The remainder of the paper is organized as follows. In section 2, we describe the system model for clipped O-OFDM. Section 3 provides a statistical analysis of clipped O-OFDM, along with analytical models. We aim to compare the performance of the proposed iterative decision-directed methods with that of SLM and ACO-SCFDE, therefore, a brief overview of SLM and ACO-SCFDE/DFT-ACO-spread has been presented in section 4. Section 5 explains TDCSR and FDCDR for clipping mitigation in details. Section 6 presents a number of simulations on the performance of the proposed methods considering both DCO- and ACO-OFDM. Moreover, the complexity implications of TDCSR and FDCDR have been discussed in section 6. Finally, Section 7 draws conclusions.

2. System Model for Clipped Optical-OFDM

Consider an O-OFDM transmission with N sub-carriers, where the frequency-domain data-symbol vector, $\boldsymbol{\mathcal{X}}$, is modulated according to M-ary QAM constellation. Here, we focus on the two state-of-the-art O-OFDM modulation techniques; DCO- and ACO-OFDM, which differs inherently in the way how the data-symbols are assigned to different sub-carriers. For clarity of exposition, the frame structure of data-symbol vector for both DCO- and ACO-OFDM has been provided. In DCO-OFDM, the sub-carriers in the frequency-domain data-symbol are arranged as $\boldsymbol{\mathcal{X}}^{(\text{D})} = \left[0, \mathcal{X}_1^{(\text{D})}, \mathcal{X}_2^{(\text{D})}, \cdots, \mathcal{X}_{N/2-1}^{(\text{D})}, 0, \mathcal{X}_{N/2-1}^{*(\text{D})}, \cdots, \mathcal{X}_2^{*(\text{D})}, \mathcal{X}_1^{*(\text{D})}\right]^{\text{T}}$. In ACO-OFDM, only odd sub-carriers carry data, i.e., $\boldsymbol{\mathcal{X}}^{(\text{A})} = \left[0, \mathcal{X}_1^{(\text{A})}, 0, \mathcal{X}_3^{(\text{A})}, \cdots, 0, \mathcal{X}_{N/2-1}^{(\text{A})}, 0, \mathcal{X}_{N/2-1}^{*(\text{A})}, \cdots, 0, \mathcal{X}_3^{*(\text{A})}, 0, \mathcal{X}_1^{*(\text{A})}\right]^{\text{T}}$. The superscripts $(\cdot)^{(\text{D})}$ and $(\cdot)^{(\text{A})}$, are used to indicate DCO- and ACO-OFDM, respectively. Hereafter, for simplicity, we have omitted the superscripts distinguishing between DCO- and ACO-OFDM, however, $\boldsymbol{\mathcal{X}}$ can use the frame structure of either. Time-domain O-OFDM signal, $\boldsymbol{x} = [x_0, x_1, \cdots, x_{N-1}]^{\text{T}}$, is generated using an N-order inverse DFT (IDFT) operation on the frequency-domain signal, $\boldsymbol{\mathcal{X}} = [\mathcal{X}_0, \mathcal{X}_1, \cdots, \mathcal{X}_{N-1}]^{\text{T}}$ as

$$x_n = \text{IDFT}\left\{\mathcal{X}_k\right\} = \frac{1}{\sqrt{N}} \sum_{k=0}^{N-1} \mathcal{X}_k \exp\left(j\frac{2\pi}{N}kn\right), \quad n = 0, \cdots, N-1 \tag{1}$$

where $j = \sqrt{-1}$, and N is the IDFT size which is considered to be equal to the number of sub-carriers. The time-domain O-OFDM signal in IM-DD is necessitated to be real-valued and non-negative. Therefore, the Hermitian symmetry property of IDFT, i.e., $\mathcal{X}_k = \mathcal{X}_{N-k}^*, 1 \leq k \leq N-1$ and $\mathcal{X}_k \in \mathfrak{Re}$, for $k = 0, N/2$, has been exploited to obtain a real time-domain O-OFDM signal. Moreover, by exploiting the central limit theorem, for $N \to \infty$, $\boldsymbol{x}$ can be modeled as Gaussian

distributed, i.e., $\mathcal{N}(0, \sigma_x^2)$. For brevity, we use $p(x)$ to represent the probability density function (pdf) of $\boldsymbol{x}$, which is given as

$$p(x) \approx \frac{1}{\sigma_x \sqrt{2\pi}} \exp\left(-\frac{x^2}{2\sigma_x^2}\right) \tag{2}$$

where σ_x^2 is the mean power of the O-OFDM signal evaluated as $\sigma_x^2 = E(|\boldsymbol{x}|^2)$.

PAPR is an important characteristic of O-OFDM signal and can be defined as the measure of variation of the time-domain signal about its mean and can be expressed as

$$\textbf{PAPR} = \lambda \triangleq \frac{\max\limits_{0 \le n \le N-1} \left(|x_n|^2\right)}{E\left(|x_n|^2\right)}. \tag{3}$$

The theoretical upper bound of PAPR for O-OFDM signals is $\lambda_{\max} = 3N_a(\sqrt{M}-1)/(\sqrt{M}+1)$ [26], where N_a is the number of active sub-carriers. However, this theoretical upper bound, $\lambda_{\max}$, can rarely be achieved [27]. The PAPR of an O-OFDM signal can be illustrated using complementary cumulative distribution function (CCDF), which is the probability that the PAPR of signal will exceed a given threshold value, PAPR_ε, i.e., CCDF = Pr(PAPR>PAPR_ε).

A cyclic prefix (CP) can be included in the time-domain O-OFDM signal to combat the inter-symbol and inter-carrier interference. Moreover, CP can transform the dispersive optical channel to flat fading optical channel [5, 28]. In what follows, CP has been omitted since it has negligible impact on the required electrical signal-to-noise ratio (SNR) and the spectral efficiency [5, 29].

After parallel-to-serial conversion (P/S), in order to counteract the high PAPR, the time-domain O-OFDM signal, $\boldsymbol{x}$, is subjected to amplitude clipping at given upper (ξ_{upper}) and lower (ξ_{lower}) levels, prior to the DAC stage. The clipped signal, $\boldsymbol{x}^{\text{c}} = \left[x_0^c, x_1^c, \cdots, x_{N-1}^c\right]^{\text{T}}$, is given as

$$x_n^{\text{c}} = \text{clip}\left\{x_n, \gamma\right\} = \begin{cases} \xi_{\text{upper}}, & x_n > \xi_{\text{upper}} \\ x_n, & \xi_{\text{lower}} \le x_n \le \xi_{\text{upper}} \\ \xi_{\text{lower}}, & x_n < \xi_{\text{lower}} \end{cases}, \quad n = 0, \cdots, N-1 \tag{4}$$

here we consider symmetric clipping for DCO-OFDM, i.e., $\xi_{\text{lower}} = -\xi_{\text{upper}} = \gamma\sigma_x$; and for ACO-OFDM, we have $\xi_{\text{lower}} = 0$, and $\xi_{\text{upper}} = \gamma\sigma_x$. The factor γ is referred to as the clipping ratio which determines the severity of clipping of time-domain O-OFDM signal. Furthermore, to obtain a non-negative time-domain signal for DCO-OFDM, the DC bias, β_{DC}, after clipping is set as $\beta_{\text{DC}} = |\min\left[x_n^c\right]| = |\xi_{\text{lower}}| = \xi_{\text{upper}}$ [2]. Whereas, for ACO-OFDM, the anti-symmetric property is exploited such that all the negative amplitudes are clipped to zero, i.e., $\xi_{\text{lower}} = 0$. Thus, the non-negative, real-valued intensity signal, $\boldsymbol{y} = [y_0, y_1, \cdots, y_{N-1}]^{\text{T}}$, for DCO- and ACO-OFDM,

obtained using (4) is given by

$$y_n = x_n^{\mathrm{c}} + \beta_{\mathrm{DC}} = \begin{cases} 2\xi_{\mathrm{upper}}, & x_n > \xi_{\mathrm{upper}} \\ x_n + \xi_{\mathrm{upper}}, & -\xi_{\mathrm{upper}} \leq x_n \leq \xi_{\mathrm{upper}} \\ 0, & x_n < -\xi_{\mathrm{upper}} \end{cases}, \quad n = 0, \cdots, N-1 \tag{5}$$

and

$$y_n = x_n^{\mathrm{c}} = \begin{cases} \xi_{\mathrm{upper}}, & x_n > \xi_{\mathrm{upper}} \\ x_n, & 0 \leq x_n \leq \xi_{\mathrm{upper}} \\ 0, & x_n < 0 \end{cases}, \quad n = 0, \cdots, N-1 \tag{6}$$

respectively.

In what follows, we assume perfect synchronization [2, 10, 30], and consider that the clipped time-domain O-OFDM signal, $\boldsymbol{x}^{\mathrm{c}}$, corresponds to the $\mathcal{DR}$ of the LED, as $\mathcal{DR} \triangleq \xi_{\mathrm{upper}} - \xi_{\mathrm{lower}}$, and the input limits of the DAC [2]. Non-linearity of the LED operating within its $\mathcal{DR}$ can be mitigated using digital pre-distortion [31], henceforth, a linear response of the LED is considered.

Noise is modeled as an additive white Gaussian noise (AWGN) given by $\boldsymbol{w} = [w_0, w_1, \cdots, w_{N-1}]^{\mathrm{T}}$ [7]. The light intensity is photo-detected at the receiver using a photo-detector (PD), and is electronically amplified using a trans-impedance amplifier (TIA). TIA output signal, $\hat{\boldsymbol{y}} = [\hat{y}_0, \hat{y}_1, \cdots, \hat{y}_{N-1}]^{\mathrm{T}}$, can be given as

$$\hat{\boldsymbol{y}} = h_{\mathrm{opt}}\boldsymbol{y} + \boldsymbol{w}. \tag{7}$$

where h_{opt} is the optical path gain coefficient of the channel [5]. The noise, $\boldsymbol{w}$, is assumed to be IID (independent and identically distributed) with zero mean and variance of σ_w^2. It has been considered that there is no additional clipping introduced by the PD. After N-order DFT operation on (7), the received frequency-domain symbols can be expressed as

$$\hat{\boldsymbol{\mathcal{Y}}} = h_{\mathrm{opt}}\boldsymbol{\mathcal{Y}} + \boldsymbol{\mathcal{W}} \tag{8}$$

where $\hat{\boldsymbol{\mathcal{Y}}} = \left[\hat{\mathcal{Y}}_0, \hat{\mathcal{Y}}_1, \cdots, \hat{\mathcal{Y}}_{N-1}\right]^{\mathrm{T}}$, $\boldsymbol{\mathcal{Y}} = [\mathcal{Y}_0, \mathcal{Y}_1, \cdots, \mathcal{Y}_{N-1}]^{\mathrm{T}}$ and $\boldsymbol{\mathcal{W}} = [\mathcal{W}_0, \mathcal{W}_1, \cdots, \mathcal{W}_{N-1}]^{\mathrm{T}}$ are frequency-domain counterparts of $\hat{\boldsymbol{y}}$, $\boldsymbol{y}$ and $\boldsymbol{w}$, respectively.

The naive receivers for O-OFDM disregard the presence of distortions instigated by the clipping process in (8) to obtain the estimated transmitted signal, and thus lead to degraded performance.

3. Statistical Analysis of Clipping

In this section, we statistically analyze the impact of clipping on the O-OFDM (the analysis provided here is a particular case of analysis in [5], since symmetric clipping is considered for DCO-OFDM, and only upper clipping has been analyzed for ACO-OFDM).

Furthermore, contrary to the approximation that $\boldsymbol{x}$ is Gaussian distributed, i.e., $\boldsymbol{x} \sim \mathcal{N}(0, \sigma_x^2)$, the clipped time-domain O-OFDM signal, $\boldsymbol{x}^{\mathrm{c}}$, rather follows a truncated Gaussian distribution which is referred to as $p(x^{\mathrm{c}})$. For DCO-OFDM, the distribution of $\boldsymbol{x}^{\mathrm{c}}$ will be Gaussian with positive and negative tails clipped at ξ_{upper} and ξ_{lower}, respectively. Whereas, for ACO-OFDM, $\boldsymbol{x}^{\mathrm{c}}$ follows a Gaussian distribution with positive tail clipped at ξ_{upper} and completely clipped negative side, since $\xi_{\mathrm{lower}} = 0$. $p(x^{\mathrm{c}})$ for DCO- and ACO-OFDM can be mathematically modeled as

$$p(x^{\mathrm{c}}) = \begin{cases} \frac{1}{2}\mathrm{erfc}\left(\frac{\xi_{\mathrm{upper}}}{\sigma_x\sqrt{2}}\right)\delta(x^{\mathrm{c}} - \xi_{\mathrm{upper}}), & x^c \geq \xi_{\mathrm{upper}} \\ \frac{1}{\sigma_x\sqrt{2\pi}}\exp\left(-\frac{x^2}{2\sigma_x^2}\right), & -\xi_{\mathrm{upper}} < x^c < \xi_{\mathrm{upper}} \\ \frac{1}{2}\mathrm{erfc}\left(\frac{\xi_{\mathrm{upper}}}{\sigma_x\sqrt{2}}\right)\delta(x^{\mathrm{c}} + \xi_{\mathrm{upper}}), & x^c \leq -\xi_{\mathrm{upper}} \end{cases} \tag{9}$$

and

$$p(x^{\mathrm{c}}) = \begin{cases} \frac{1}{2}\mathrm{erfc}\left(\frac{\xi_{\mathrm{upper}}}{\sigma_x\sqrt{2}}\right)\delta(x^{\mathrm{c}} - \xi_{\mathrm{upper}}), & x^c \geq \xi_{\mathrm{upper}} \\ \frac{1}{\sigma_x\sqrt{2\pi}}\exp\left(-\frac{x^2}{2\sigma_x^2}\right), & 0 < x^c < \xi_{\mathrm{upper}} \\ \frac{1}{2}\delta(x^{\mathrm{c}}), & x^c \leq 0 \end{cases}, \tag{10}$$

respectively, where $\mathrm{erfc}(\psi)$ is the complementary error function given as $\mathrm{erfc}(\psi) = 1 - \mathrm{erf}(\psi)$ with $\mathrm{erf}(\psi) = 2/\sqrt{\pi}\int_0^{\psi}\exp(-t^2)\mathrm{d}t$, and $\delta(\cdot)$ is the Dirac distribution. (9) and (10) follow directly from (4). Refer to Fig. 1 for the illustration of the pdf of clipped DCO- and ACO-OFDM, respectively. Dirac distribution, $\delta(\cdot)$, appears at the clipping thresholds for the clipped O-OFDM signals, and is multiplied by the probability of the samples to be clipped.

The power of clipped O-OFDM, $\sigma_{x^{\mathrm{c}}}^2$, can be obtained directly from the distributions of DCO- and

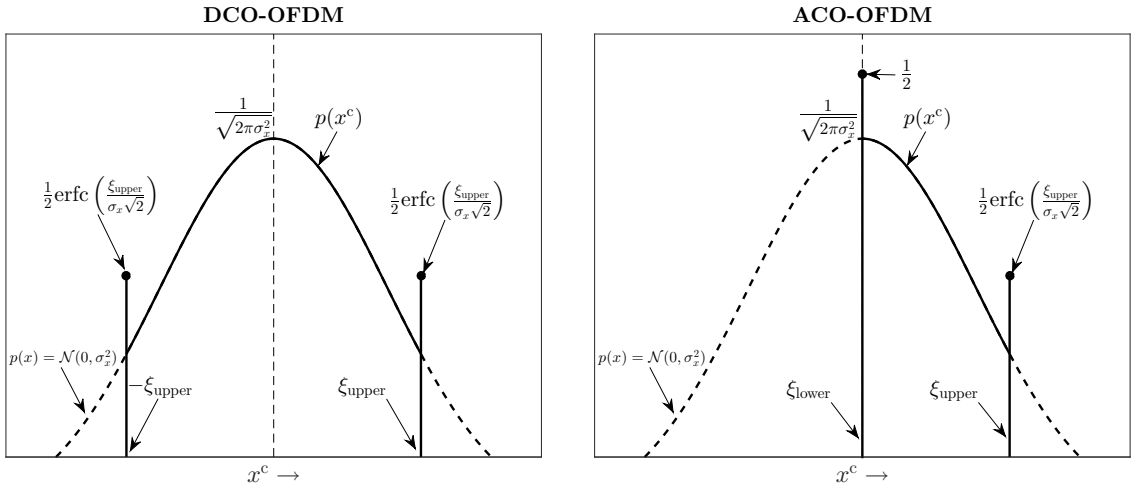

Figure 1: Illustration of probability density function of clipped DCO- and ACO-OFDM. Solid line represents the distribution of clipped DCO- and ACO-OFDM while the dashed line represents the Gaussian distribution of unclipped DCO- and ACO-OFDM.

ACO-OFDM given in (9) and (10) as

$$\begin{aligned}\sigma_{x^{\mathrm{c}}}^2 &= 2\int_0^{\xi_{\mathrm{upper}}} \frac{x^2}{\sigma_x\sqrt{2\pi}} \exp\left(-\frac{x^2}{2\sigma_x^2}\right) \mathrm{d}x + \xi_{\mathrm{upper}}^2 \mathrm{erfc}\left(\frac{\xi_{\mathrm{upper}}}{\sigma_x\sqrt{2}}\right) \\ &= \sigma_x^2\left[1 - \sqrt{\frac{2}{\pi}}\gamma \exp\left(-\frac{\gamma^2}{2}\right) - (1-\gamma^2)\mathrm{erfc}\left(\frac{\gamma}{\sqrt{2}}\right)\right],\end{aligned} \tag{11}$$

and

$$\begin{aligned}\sigma_{x^{\mathrm{c}}}^2 &= \int_0^{\xi_{\mathrm{upper}}} \frac{x^2}{\sigma_x\sqrt{2\pi}} \exp\left(-\frac{x^2}{2\sigma_x^2}\right) \mathrm{d}x + \frac{\xi_{\mathrm{upper}}^2}{2} \mathrm{erfc}\left(\frac{\xi_{\mathrm{upper}}}{\sigma_x\sqrt{2}}\right) \\ &= \frac{\sigma_x^2}{2}\left[1 - \sqrt{\frac{2}{\pi}}\gamma \exp\left(-\frac{\gamma^2}{2}\right) - (1-\gamma^2)\mathrm{erfc}\left(\frac{\gamma}{\sqrt{2}}\right)\right],\end{aligned} \tag{12}$$

respectively.

Furthermore, by applying Bussgang decomposition [32, 33] and considering that $\boldsymbol{x} \sim \mathcal{N}(0, \sigma_x^2)$, $\boldsymbol{x}^{\mathrm{c}}$ can be statistically modeled as a sum of two uncorrelated parts as

$$\boldsymbol{x}^{\mathrm{c}} = \alpha\boldsymbol{x} + \boldsymbol{d} \tag{13}$$

where α is a linear attenuation factor, and $\boldsymbol{d}$ is the clipping distortion, statistically uncorrelated to $\boldsymbol{x}$, i.e., $E(\boldsymbol{d}\boldsymbol{x}^*) = 0$. The linear attenuation factor, α, is a function of non-linear distortion, which in this case, is clipping. Moreover, α can be evaluated by exploiting the Bussgang Theorem [33], as

$$\alpha = \frac{\mathrm{cov}\left[\boldsymbol{x}, \boldsymbol{x}^{\mathrm{c}}\right]}{\sigma_x^2} = \frac{1}{2}\mathrm{erf}\left(\frac{\xi_{\mathrm{upper}}}{\sigma_x\sqrt{2}}\right) - \frac{1}{2}\mathrm{erf}\left(\frac{\xi_{\mathrm{lower}}}{\sigma_x\sqrt{2}}\right). \tag{14}$$

α reflects the shrinkage of the signal amplitude caused by signal clipping. From (14), the power dissipation due to attenuation factor, α^2, for DCO- and ACO-OFDM can be given as

$$\alpha^2 = \begin{cases} \mathrm{erf}^2\left(\frac{\gamma}{\sqrt{2}}\right), & \text{for DCO-OFDM} \\ \frac{1}{4}\mathrm{erf}^2\left(\frac{\gamma}{\sqrt{2}}\right), & \text{for ACO-OFDM.} \end{cases} \tag{15}$$

Furthermore, owing to (13), the modified power of the time-domain O-OFDM can be given as

$$\sigma_{x^{\mathrm{c}}}^2 = \alpha^2\sigma_x^2 + \sigma_{\mathrm{d}}^2 \tag{16}$$

where σ_{d}^2 is the power of instigated distortions. Considering DCO-OFDM, the distortions is clipping of the time-domain DCO-OFDM signal, therefore, the power of clipping distortion is given as $\sigma_{\mathrm{c}}^2 = \sigma_{\mathrm{d}}^2$. Whereas, for ACO-OFDM, the distortions are instigated because of clipping of time-domain ACO-OFDM signal, and moreover, the clipping process induces a DC component which is irrelevant to the clipping noise variance on the data-carrying sub-carriers, thus, we have $\sigma_{\mathrm{c}}^2 = \sigma_{\mathrm{d}}^2 - \sigma_{\mathrm{DC}}^2$, where σ_{DC}^2 is the power of the DC component. So, the power of clipping distortion for DCO- and ACO-

OFDM can be given as

$$\begin{aligned}\sigma_{\mathrm{c}}^2 &= \alpha^2\sigma_x^2 + \sigma_{x^{\mathrm{c}}}^2 \\ &= \sigma_x^2\left[1 - \mathrm{erf}^2\left(\frac{\gamma}{\sqrt{2}}\right) - \sqrt{\frac{2}{\pi}}\gamma\exp\left(-\frac{\gamma^2}{2}\right) - (1-\gamma^2)\mathrm{erfc}\left(\frac{\gamma}{\sqrt{2}}\right)\right],\end{aligned} \tag{17}$$

and

$$\begin{aligned}\sigma_{\mathrm{c}}^2 &= \alpha^2\sigma_x^2 + \sigma_{x^{\mathrm{c}}}^2 - \sigma_{\mathrm{DC}}^2 \\ &= \frac{\sigma_x^2}{2}\left[1 - \frac{1}{2}\mathrm{erf}^2\left(\frac{\gamma}{\sqrt{2}}\right) - \sqrt{\frac{2}{\pi}}\gamma\exp\left(-\frac{\gamma^2}{2}\right) - (1-\gamma^2)\mathrm{erfc}\left(\frac{\gamma}{\sqrt{2}}\right)\right] - \underbrace{\left\{\int_0^{\xi_{\mathrm{upper}}} x^{\mathrm{c}}p(x^{\mathrm{c}})\mathrm{d}x^{\mathrm{c}}\right\}^2}_{:=\text{DC Component}} \\ &= \frac{\sigma_x^2}{2}\left[1 - \frac{1}{2}\mathrm{erf}^2\left(\frac{\gamma}{\sqrt{2}}\right) - \frac{1}{\pi}\left\{1-\exp\left(-\frac{\gamma^2}{2}\right)\right\}^2 - \sqrt{\frac{2}{\pi}}\gamma\exp\left(-\frac{\gamma^2}{2}\right) - (1-\gamma^2)\mathrm{erfc}\left(\frac{\gamma}{\sqrt{2}}\right)\right],\end{aligned} \tag{18}$$

respectively. Note that the attenuation factor, α, and variance of clipping distortion, σ_{c}^2, are independent of the QAM constellation order, M, and the IDFT/DFT size, N, however, are a function of clipping ratio, γ.

Using (17), (18), considering the impact of AWGN and perfect equalization, an analytical expression for the effective SNR, κ, for O-OFDM, similar to the one in [5], can be obtained as

$$\kappa = \frac{\alpha^2\sigma_x^2/\zeta_{\mathrm{B}}}{\sigma_{\mathrm{c}}^2 + \sigma_w^2\zeta_{\mathrm{B}}/(h_{\mathrm{opt}}\zeta_{\mathrm{DC}})}, \tag{19}$$

when the power of the enabled sub-carriers is scaled to $\sigma_x^2/\zeta_{\mathrm{B}}$, with ζ_{B} being the utilization factor of double sided bandwidth, B given as

$$\zeta_{\mathrm{B}} = \begin{cases} \frac{N-2}{N}, & \text{for DCO-OFDM} \\ \frac{1}{2}, & \text{for ACO-OFDM.} \end{cases} \tag{20}$$

Moreover, ζ_{DC} represents the attenuation of the useful electrical signal power due to the DC bias and is given as

$$\zeta_{\mathrm{DC}} = \begin{cases} \frac{1}{1+\gamma^2}, & \text{for DCO-OFDM} \\ 1, & \text{for ACO-OFDM.} \end{cases} \tag{21}$$

$\zeta_{\mathrm{DC}} = 1$ for ACO-OFDM, follows from the fact that no DC bias has been considered. Furthermore, (19) represents the ratio between the attenuated signal power and total noise power per symbol. Moreover, for simplicity, we consider $h_{\mathrm{opt}} = 1$. Once κ is evaluated using (19), exact closed-form

expressions for the BER performance of M-ary QAM in AWGN, can be used to evaluate the BER behaviour of O-OFDM under different clipping conditions. The analytical closed-form expression for the BER performance of M-ary QAM O-OFDM is given as [5]

$$\mathrm{BER} = \frac{2(\sqrt{M}-1)}{\sqrt{M}\log_2(M)}\mathrm{erfc}\left(\sqrt{\frac{3\log_2(M)}{M-1}}\kappa\right) + \frac{2(\sqrt{M}-2)}{\sqrt{M}\log_2(M)}\mathrm{erfc}\left(3\sqrt{\frac{3\log_2(M)}{M-1}}\kappa\right). \tag{22}$$

Hereafter, we refer to the model described in this section as 'analytical model'.

4. Review of Selected-Mapping (SLM) and Asymmetrically Clipped Optical-SCFDE (ACO-SCFDE)

We intend to compare the performance of proposed decision-directed PAPR reduction methods with standard methods available in the literature. For a fair comparison, techniques with similar spectral efficiencies are adopted. For DCO-OFDM, we compare the performance of proposed methods which that of SLM. To the best of our knowledge, no SCFDE technique is available in literature which has a same spectral efficiency as that of DCO-OFDM, therefore, the comparison is restricted to the classical SLM. Whereas, for ACO-OFDM, we compare the performance of the proposed methods with that of SLM (since SLM can be adopted for spectral efficiency equal to that of ACO-OFDM) and ACO-SCFDE. For the sake of understanding, a brief overview of both SLM and ACO-SCFDE is provided.

4.1. Selected-Mapping (SLM)

The block diagram of selected-mapping (SLM) is provided in Fig. 2 and the technique has been adopted for IM-DD in [10]. In SLM, a set of $\mathcal{U}$ statistically independent candidate signals, representing the same information is generated at the transmitter. The most favourable signal as regards to minimum PAPR is chosen to be transmitted. $\mathcal{U}$ signals are obtained such that the frequency-domain data-symbol vector, $\boldsymbol{\mathcal{X}} = [\mathcal{X}_0, \mathcal{X}_1, \cdots, \mathcal{X}_{N-1}]^{\mathrm{T}}$, which is constrained to have Hermitian symmetry is weighted by $\mathcal{U}$ distinct phase sequences, $\boldsymbol{\mathcal{P}}^{(u)} = \left[\mathcal{P}_0^{(u)}, \mathcal{P}_1^{(u)}, \cdots, \mathcal{P}_{N-1}^{(u)}\right]^{\mathrm{T}}$, where $u = 1, 2, \cdots, \mathcal{U}$, to produce a modified data-block, $\boldsymbol{\mathcal{R}}^{(u)} = \left[\mathcal{R}_0^{(u)}, \mathcal{R}_1^{(u)}, \cdots, \mathcal{R}_{N-1}^{(u)}\right]^{\mathrm{T}}$. The elements of phase vector, $\boldsymbol{\mathcal{P}}^{(u)}$ are also chosen such that the Hermitian symmetry of the data-symbol vector is preserved. Therefore, $N/2-1$ elements of phase vector are chosen randomly and uniformly from the set $\{-1, +1\}$. Moreover, all elements of $\boldsymbol{\mathcal{P}}^{(1)}$ are set to 1, in order to accommodate the original data-symbol vector, as a result, the degree of freedom of choice of phase sequences, $\boldsymbol{\mathcal{P}}^{(u)}$, is $\mathcal{U}-1$. IDFT of $\mathcal{U}$ independent sequences $\boldsymbol{\mathcal{R}}^{(u)}$ are taken to produce the sequences $\boldsymbol{r}^{(u)} = \left[r_0^{(u)}, r_1^{(u)}, \cdots, r_{N-1}^{(u)}\right]^{\mathrm{T}}$, from which the PAPR, $\lambda^{(u)}$, of each sequence, $\boldsymbol{r}^{(u)}$ is evaluated. The sequence which gives the minimum $\lambda^{(u)}$, referred to as $\boldsymbol{x}$ is chosen to be transmitted. Further, in order to recover original data block at the receiver, information about the chosen phase vector needs to be explicitly transmitted along with the chosen signal, $\boldsymbol{x}$. Since a set of $\mathcal{U}$ statistically independent candidate signals is considered, SLM technique requires $\mathcal{U}$ times N-order IDFT computations, while

the number of bits required for transmitted side information is $\log_2\lfloor \mathcal{U} \rfloor$, where $\log_2\lfloor z \rfloor$ denotes the greatest integer less than z. The PAPR reduction for SLM depends on the number of phase vectors, $\mathcal{U}$. Increasing the number of phase vectors, results in an increase in peak power reduction, however, on the other hand also results in an increase in the number of IDFT computations. Note that, the goal of SLM is to make the occurrence of the peaks less frequent rather to eliminate the peaks altogether. SLM can be adopted for any number of sub-carriers, however, the overhead of side information needs to be transmitted to the receiver along with the signal[1].

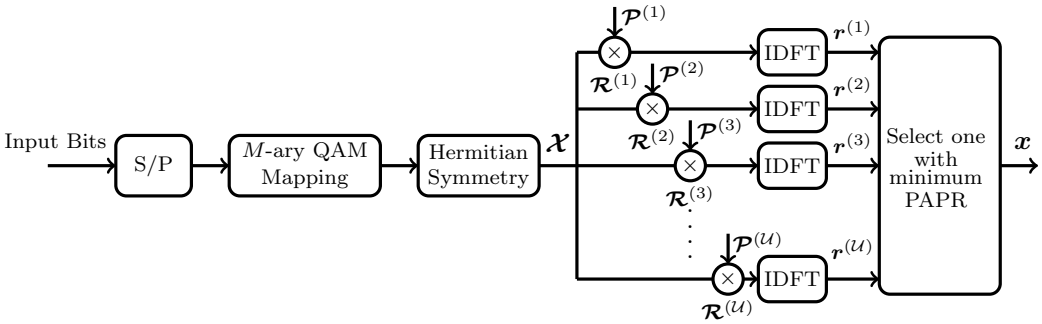

Figure 2: Block diagram of selected-mapping (SLM) technique.

4.2. Asymmetrically Clipped Optical-SCFDE (ACO-SCFDE)

Asymmetrically Clipped Optical-SCFDE (ACO-SCFDE) can be considered as the SCFDE counterpart of ACO-OFDM and was proposed for IM-DD in [13]. The block diagram of ACO-SCFDE is presented in Fig. 3. At the transmitter, a set of $N/4$ complex data-symbols are chosen according to M-ary QAM, and is denoted by $\boldsymbol{s} = \left[s_0, s_1, \cdots, s_{N/4-1}\right]^{\mathrm{T}}$. $N/4$-order DFT is performed on $\boldsymbol{s}$ to achieve a frequency-domain data-symbol vector, $\boldsymbol{\mathcal{S}} = \left[\mathcal{S}_0, \mathcal{S}_1, \cdots, \mathcal{S}_{N/4-1}\right]^{\mathrm{T}}$. $N/4$ complex symbols of $\boldsymbol{\mathcal{S}}$ are mapped to a Hermitian symmetric vector of length $N/2$, which is then interleaved with zeros to obtain the frequency-domain data-symbol vector of length N, which only carries data on the odd indexes, i.e., $\boldsymbol{\mathcal{X}} = \left[0, \mathcal{S}_0, 0, \mathcal{S}_1, \cdots, 0, \mathcal{S}_{N/4-1}, 0, \mathcal{S}^*_{N/4-1}, \cdots, 0, \mathcal{S}^*_1, 0, \mathcal{S}^*_0\right]^{\mathrm{T}}$. Note that $N/4$-order DFT process prior to obtaining frequency-domain data-symbol vector is similar to DFT-spread operation. N-order IDFT operation is performed, to generate a real time-domain SCFDE signal $\boldsymbol{x} = [x_0, x_1, \cdots, x_{N-1}]^{\mathrm{T}}$. Because of symbol arrangement in $\boldsymbol{\mathcal{X}}$, the signal $\boldsymbol{x}$ will be anti-symmetric, i.e., $x_n = -x_{n+N/2}, 0 \leq n \leq N/2-1$, the negative part of which can be clipped without any loss of useful information, to obtain a non-negative real signal, $\boldsymbol{y} = [y_0, y_1, \cdots, y_{N-1}]^{\mathrm{T}}$, which is then modulated onto the intensity of the LED. At the receiver, the signal is photo-detected using a PD and is converted to an electrical signal, $\hat{\boldsymbol{y}} = [\hat{y}_0, \hat{y}_1, \cdots, \hat{y}_{N-1}]^{\mathrm{T}}$. An N-order DFT is applied on $\hat{\boldsymbol{y}}$, to obtain a frequency-domain data-symbol vector, $\hat{\boldsymbol{\mathcal{Y}}}$, from which the odd sub-carriers are

[1]In our implementation of SLM, we consider that the phase vector of the chosen lowest PAPR signal is known to the receiver.

extracted, exactly as in ACO-OFDM, to yield, $\boldsymbol{\mathcal{R}} = 1/2\left[\mathcal{S}_0, \mathcal{S}_1, \cdots, \mathcal{S}_{N/4-1}, \mathcal{S}^*_{N/4-1}, \cdots, \mathcal{S}^*_1, \mathcal{S}^*_0\right]^{\mathrm{T}}$. After that, $\boldsymbol{\mathcal{R}}$ is transformed into time-domain signal, $\boldsymbol{r} = \left[r_0, r_1, \cdots, r_{N/4-1}\right]^{\mathrm{T}}$ using an $N/4$-order IDFT, and decisions on the symbols are made based on $\boldsymbol{r}$. Note that the spectral efficiency of ACO-SCFDE is same as that of ACO-OFDM. The main difference between ACO-SCFDE and ACO-OFDM is the additional $N/4$-order DFT and IDFT transforms at both the transmitter and the receiver, which converts the scheme from multi-carrier to single carrier transmission, and therefore, exhibits a lower PAPR compared to ACO-OFDM[2].

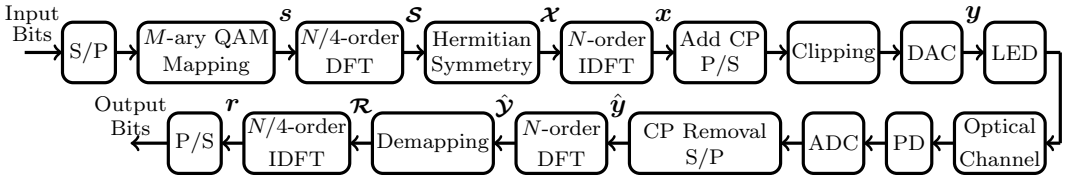

Figure 3: Block diagram of asymmetrically clipped optical SCFDE (ACO-SCFDE).

5. Proposed TDCSR and FDCDR Methods

Two iterative decision-directed methods for PAPR reduction for O-OFDM are presented in this section. A block diagram explaining how the proposed decision-directed methods can be employed in an O-OFDM systems is given in Fig. 4. It is important to note that before clipping mitigation, the received unipolar O-OFDM signals have to be converted to bipolar signals by removing the DC bias in DCO-OFDM, and by exploiting the anti-symmetric property to recover the negative samples in ACO-OFDM. Note that the set of received frequency-domain symbols, $\hat{\boldsymbol{\mathcal{Y}}}$, is equalized in case of dispersive channel for both TDCSR and FDCDR.

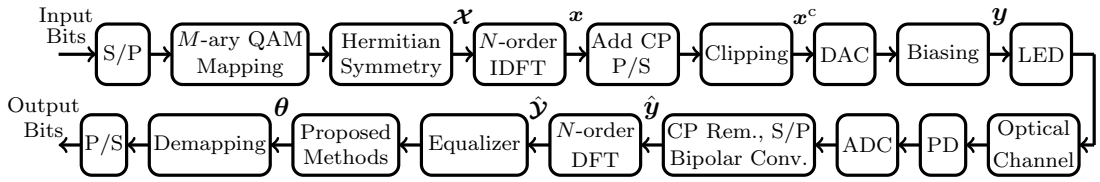

Figure 4: Block diagram of an O-OFDM system explaining how the proposed iterative decision-directed methods can be employed.

[2]ACO-SCFDE [13] and ACO-DFT-spread [14] are exactly similar in their implementation. As a consequence, the performance of ACO-SCFDE is similar to that of ACO-DFT-spread, both in terms of BER and PAPR reduction. Moreover, in [14], along with the DFT-spread operation for ACO-OFDM, i.e., ACO-DFT-spread, the authors have used clipping to to further reduce the PAPR. However, ACO-SCFDE/ACO-DFT-spread considered here has no additional clipping.

5.1. Time-Domain Clipped Sample Reconstruction (TDCSR)

In time-domain clipped sample reconstruction (TDCSR), clipping is mitigated by reconstructing the affected samples in the time-domain. The iterative structure of TDCSR is given in Fig. 5, and the iterative process is presented as follows:

(1) The received reference O-OFDM time-domain signal, $\hat{\boldsymbol{r}}$, is obtained from the set of received frequency-domain symbols, $\hat{\boldsymbol{\mathcal{Y}}}$, as $\hat{\boldsymbol{r}} = \text{IDFT}\{\hat{\boldsymbol{\mathcal{Y}}}\}$, and is then buffered. This step is performed only once, and is therefore not a part of iterative structure of TDCSR shown in Fig. 5.

(2) Decisions for the ith iteration are made on $\boldsymbol{\theta}^{(i)}$ in frequency-domain to obtain a set of retrieved symbols, $\hat{\boldsymbol{\theta}}^{(i)} = \text{Slicer}\{\boldsymbol{\theta}^{(i)}\}$, where Slicer$\{\cdot\}$ represents a hard symbol estimator. For the first iteration, $i = 1$, we have $\boldsymbol{\theta}^{(1)} = \hat{\boldsymbol{\mathcal{Y}}}$, i.e., the set of received frequency-domain symbols, $\hat{\boldsymbol{\mathcal{Y}}}$, are used to seed the TDCSR iterative process.

(3) The symbol set, $\hat{\boldsymbol{\theta}}^{(i)}$, is then converted to time-domain to obtain an estimated O-OFDM signal, $\hat{\boldsymbol{s}}^{(i)}$, evaluated as $\hat{\boldsymbol{s}}^{(i)} = \text{IDFT}\{\hat{\boldsymbol{\theta}}^{(i)}\}$. The conversion of frequency-domain symbols, $\hat{\boldsymbol{\theta}}^{(i)}$, to time-domain O-OFDM signal, $\hat{\boldsymbol{s}}^{(i)}$, significantly mitigates the clipping noise because of peak regrowth of clipped samples in $\hat{\boldsymbol{s}}^{(i)}$. The peak regrowth has been depicted in Fig. 6. Hence, this peak regrowth in $\hat{\boldsymbol{s}}^{(i)}$ can be exploited to reconstruct the affected clipped samples $\hat{\boldsymbol{r}}$.

(4) The clipped samples in $\hat{\boldsymbol{r}}$ are identified by recreating a similar clipping process as at the transmitter, considering that clipping ratio, γ, is known at the receiver.

(5) The identified clipped samples in $\hat{\boldsymbol{r}}$, are then substituted with corresponding samples from $\hat{\boldsymbol{s}}^{(i)}$, resulting in a reconstructed time-domain O-OFDM signal, $\tilde{\boldsymbol{r}}^{(i)}$, given as

$$\tilde{r}_n^{(i)} = \begin{cases} \hat{s}_n^{(i)} & \hat{s}_n^{(i)} > \xi_{\text{upper}} \\ \hat{r}_n & \xi_{\text{lower}} \leq \hat{s}_n^{(i)} \leq \xi_{\text{upper}} \\ \hat{s}_n^{(i)} & \hat{s}_n^{(i)} < \xi_{\text{lower}} \end{cases} \tag{23}$$

where $\hat{r}_n$ and $\hat{s}_n^{(i)}$ are the nth elements of $\hat{\boldsymbol{r}}$ and $\hat{\boldsymbol{s}}^{(i)}$, respectively.

(6) The reconstructed time-domain O-OFDM signal, $\tilde{\boldsymbol{r}}^{(i)}$, is converted to frequency-domain symbols as $\boldsymbol{\theta}_r^{(i)} = \text{DFT}\{\tilde{\boldsymbol{r}}^{(i)}\}$, and hence a new set of reconstructed symbols, $\boldsymbol{\theta}_r^{(i)}$, is obtained.

(7) Iteration counter is incremented, $i = i + 1$, and $\boldsymbol{\theta}^{(i)}$ is updated as $\boldsymbol{\theta}^{(i)} = \boldsymbol{\theta}_r^{(i-1)}$ which is then used as an input to the following iteration to further refine the time-domain reconstruction process.

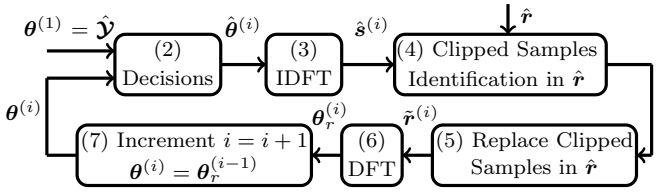

Figure 5: Iterative structure for time-domain clipped sample reconstruction (TDCSR).

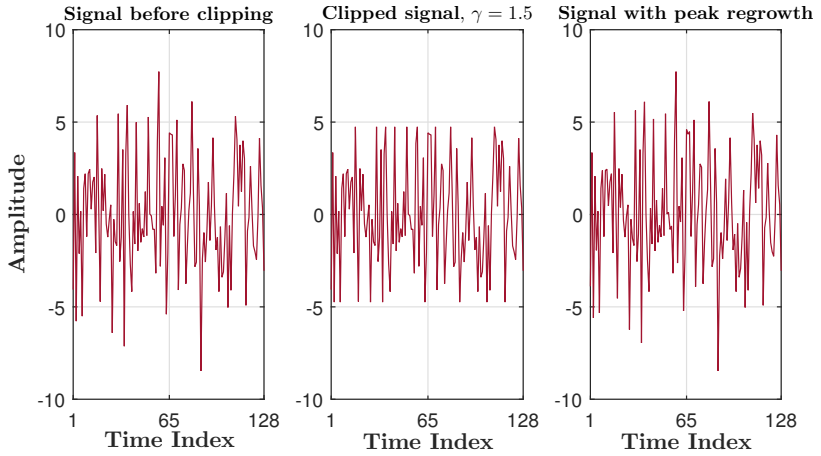

Figure 6: Illustration of peak regrowth (noiseless scenario) of clipped samples as described in step (3) of TDCSR. DCO-OFDM with 16-QAM constellation and $N = 128$ is used.

5.2. Frequency-Domain Clipping Distortion Removal (FDCDR)

In frequency-domain clipping distortion removal (FDCDR), clipping mitigation is achieved by means of clipping distortion cancellation in the frequency-domain. The iterative structure for FDCDR is presented in Fig. 7, and the technique is explained as follows:

(1) Decisions for the ith iteration are made on $\boldsymbol{\theta}^{(i)}$, to obtain a set of retrieved symbols, $\hat{\boldsymbol{\theta}}^{(i)} = \text{Slicer}\{\boldsymbol{\theta}^{(i)}\}$. For the first iteration, $i = 1$, which seeds the algorithm, clipping distortion contribution is neglected, i.e., $\boldsymbol{\mathcal{D}}^{(1)} = 0$, and the received frequency-domain symbols, $\hat{\boldsymbol{\mathcal{Y}}}$, are used as an input to the FDCDR iterative process, i.e., $\boldsymbol{\theta}^{(1)} = \hat{\boldsymbol{\mathcal{Y}}}$.

(2) An estimated time-domain O-OFDM signal, $\hat{\boldsymbol{s}}^{(i)}$, is obtained via $\hat{\boldsymbol{s}}^{(i)} = \text{IDFT}\{\hat{\boldsymbol{\theta}}^{(i)}\}$.

(3) Assuming that the clipping ratio is known at the receiver, $\hat{\boldsymbol{s}}^{(i)}$ is subjected to a similar clipping process as at the transmitter to generate a clipped time-domain O-OFDM signal, $\hat{\boldsymbol{c}}^{(i)}$.

(4) The clipped version of $\hat{\boldsymbol{\theta}}^{(i)}$, $\hat{\boldsymbol{\theta}}_c^{(i)}$, is obtained as $\hat{\boldsymbol{\theta}}_c^{(i)} = \text{DFT}\{\hat{\boldsymbol{c}}^{(i)}\}$. By mimicking a similar clipping process as at the transmitter as done in step (3), a distortion, $\boldsymbol{\mathcal{D}}^{(i)}$, similar to the one introduced at the transmitter is now instigated in $\hat{\boldsymbol{\theta}}_c^{(i)}$, where $\hat{\boldsymbol{\theta}}_c^{(i)} = \hat{\boldsymbol{\theta}}^{(i)} + \boldsymbol{\mathcal{D}}^{(i)}$.

(5) An estimate of the clipping distortion component, $\boldsymbol{\mathcal{D}}^{(i)}$, can be made by subtracting $\hat{\boldsymbol{\theta}}_c^{(i)}$ from $\hat{\boldsymbol{\theta}}^{(i)}$, as $\boldsymbol{\mathcal{D}}^{(i)} = \hat{\boldsymbol{\theta}}_c^{(i)} - \hat{\boldsymbol{\theta}}^{(i)}$.

(6) Iteration counter is incremented $i = i + 1$.

(7) The input for the next iteration is updated as $\boldsymbol{\theta}^{(i)} = \boldsymbol{\theta}^{(i-1)} - \boldsymbol{\mathcal{D}}^{(i-1)}$, i.e., by removing the estimated clipping distortion from the set of retrieved symbols.

(8) Updated $\boldsymbol{\theta}^{(i)}$ is used in successive iteration to obtain a better estimate of the clipping distortion component.

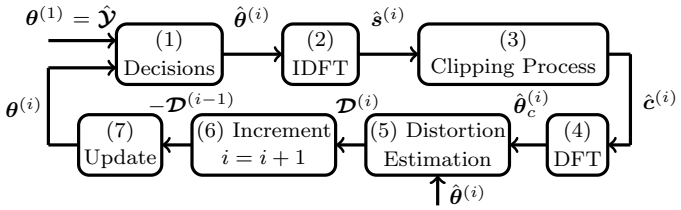

Figure 7: Iterative structure for frequency-domain clipping distortion removal (FDCDR).

6. Performance Analysis of TDCSR and FDCDR

6.1. Simulation Results

In this section, simulation results are presented to demonstrate and compare the performance of TDCSR and FDCDR with other PAPR reduction methods available in the literature, such as SLM [10] and ACO-SCFDE [13]. Unless otherwise mentioned, constellation of type 16-QAM (64- and 256-QAM are only considered for power efficiency analysis) and 3 iterations for the decision-directed methods are considered. Simulation results are also provided when uniform quantization is considered for O-OFDM. Performance of TDCSR and FDCDR as a function of different number of iterations for the iterative structure has also been investigated. Complementary cumulative distribution function (CCDF) curves are presented to illustrate the PAPR of the O-OFDM signals. Further, power efficiency analysis is realized for both TDCSR and FDCDR considering DCO- and ACO-OFDM, and is also compared with power efficiencies of conventional DCO-, ACO-OFDM (without clipping), SLM and ACO-SCFDE. Note that, for TDCSR and FDCDR, the minimum clipping ratio for 4-, 16-, 64- and 256-QAM is recommended as 1, 1.4, 1.9 and 2.5, respectively, for DCO-OFDM, and 0.7, 1.1, 1.6 and 2.3, respectively, for ACO-OFDM[3]. DCO- and ACO-OFDM with 1024 sub-carriers are simulated, and the results are averaged over 2000 independent OFDM/SCFDE realizations.

6.1.1. Bit Error Rate Performance

First, we evaluate the BER performance of TDCSR and FDCDR considering DCO-OFDM and clipping ratios of 1.5 and 1.8. The BER performance for TDCSR and FDCDR is depicted in Fig. 8, and is compared with SLM using $\mathcal{U} = 128$ phase vectors [10]. The number phase vectors for SLM considered here are significantly high, therefore, SLM performance depicted here can be considered as an upper-bound on the scheme's performance. Conventional DCO-OFDM with $\beta_{\text{DC}} = 7$ dB is used as a benchmark [1] and further, the analytical BER to validate the simulation model for clipped DCO-OFDM is also provided. Clearly, both TDCSR and FDCDR achieve a significant gain

[3]The recommended range of clipping ratios for TDCSR and FDCDR, at which the clipping distortion can be mitigated, is determined by performing simulations with a broad variety of systems setup, and considering a target BER of 10^{-3} and 3 iterations of the iterative structure. Once the recommended range is determined, we take a clipping ratio within the recommended range for the simulations.

over conventional DCO-OFDM, whereas, a marginal gain is observed over SLM. The performance gain for TDCSR and FDCDR over conventional DCO-OFDM is expected, because due to signal clipping, the required DC bias, β_{DC}, has been reduced from 7 dB to 5.1 dB for $\gamma = 1.5$, and from 7 dB to 6.3 dB for $\gamma = 1.8$. More importantly, it has been demonstrated in Fig. 9, that the reduction incurred in PAPR is approximately equal to 7.2 dB and 5.7 dB for γ of 1.5 and 1.8, respectively, whereas with SLM, PAPR is reduced by approximately 2.2 dB when $\mathcal{U} = 128$. PAPR reduction for SLM using $\mathcal{U} = 6$ (not presented here) is only 1.3 dB, which is insignificant.

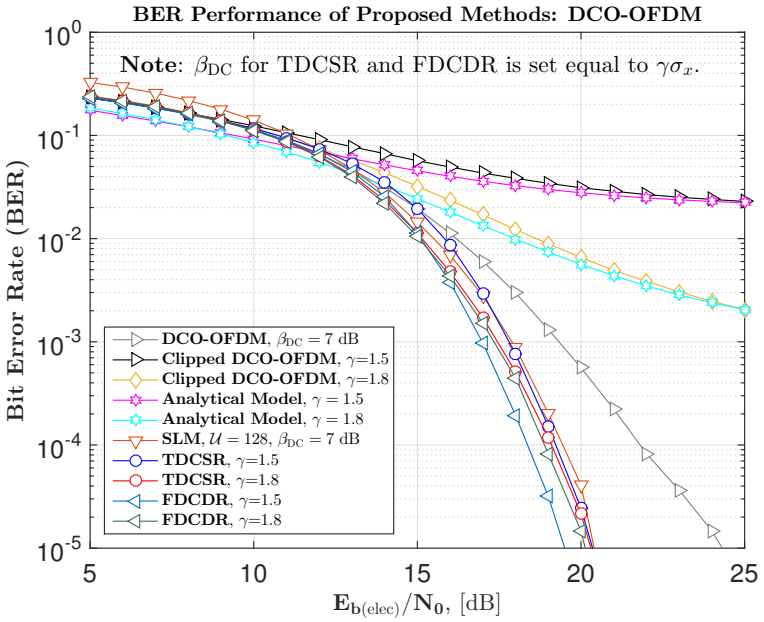

Figure 8: BER comparison of clipped DCO-OFDM, clipped DCO-OFDM with clipping mitigation using TDCSR and FDCDR, and SLM with $\mathcal{U} = 128$ for 16-QAM constellation and $N = 1024$. The analytical model for clipped DCO-OFDM is presented in Sec. 3.

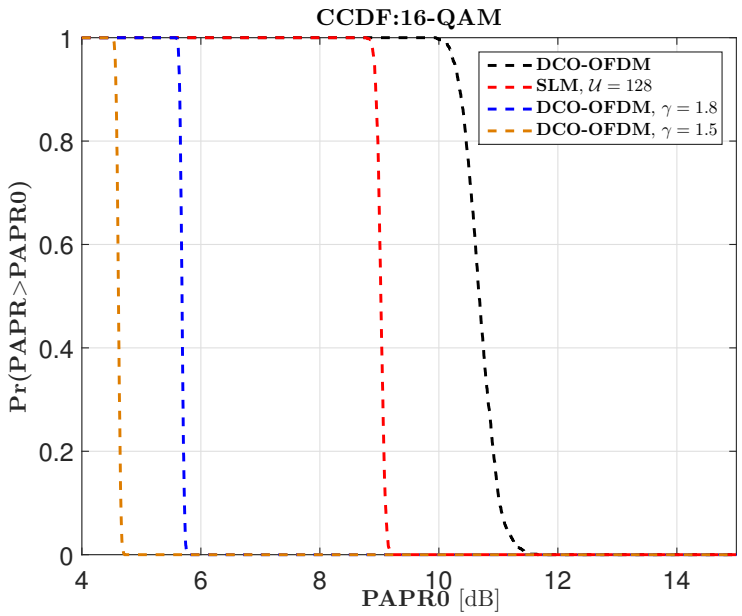

Figure 9: CCDF of PAPR comparison of clipped DCO-OFDM, DCO-OFDM and SLM with $\mathcal{U} = 128$. The clipping ratios, γ, used for clipped DCO-OFDM are 1.5 and 1.8.

We now move on assessing the BER performance of TDCSR and FDCDR for ACO-OFDM, which has been depicted in Fig. 10. The clipping ratios are set equal to 1.2 and 1.3. Conventional ACO-OFDM is used as reference, and the performance of the proposed methods is compared with that of ACO-SCFDE and SLM with $\mathcal{U} = 128$. Analytical model has been provided for the clipped ACO-OFDM signal to validate the clipping model used in simulations. Compared to the BER performance of ACO-SCFDE and SLM, TDCSR exhibits a comparable performance, whereas, there exists a marginal performance loss for FDCDR. Note that the performance gain of using the proposed methods with ACO-OFDM is significant over conventional ACO-OFDM and ACO-SCFDE, if clipping is applied to fit the time-domain signal in the limited dynamic range of the LED. Moreover, TDCSR outperforms FDCDR because at each iteration, two time-domain samples are reconstructed to provide distortion compensation for one useful frequency-domain symbol, owing to the time-domain anti-symmetric property of ACO-OFDM [7]. It can also be established that the PAPR can be drastically reduced using signal clipping, see Fig. 11. Note that the reduction in PAPR is a function of the clipping ratio, smaller values of clipping ratio within the recommended range for the proposed methods would result in a significantly lower PAPR compared to both ACO-SCFDE and SLM, as it can be seen in Fig. 11. PAPR reduction by signal clipping is approximately equal to 5.6 dB and 5.3 dB for γ of 1.2 and 1.3, respectively, whereas, ACO-SCFDE can reduce the PAPR by approximately 1.8 dB, and SLM by 2.3 dB. Furthermore, it can also be concluded that the PAPR reduction using clipping is significant as compared when DHT-spread based ACO-OFDM with similar data rate is considered [17, 18]. Large reduction in PAPR is important in practical

systems, where the performance of the system is also limited by limited bit resolution DAC. A smaller signal range will result in much reduced quantization noise and also relax the bit resolution requirement of the DAC. Moreover, clipping also increase the modulation power by approximately 3.8 dB and 3.5 dB for clipped ACO-OFDM using γ of 1.2 and 1.3, respectively, compared to conventional ACO-OFDM at the output of DAC to drive the LED. In the subsequent subsection, the performance of TDCSR and FDCDR considering the quantization noise has been analysed.

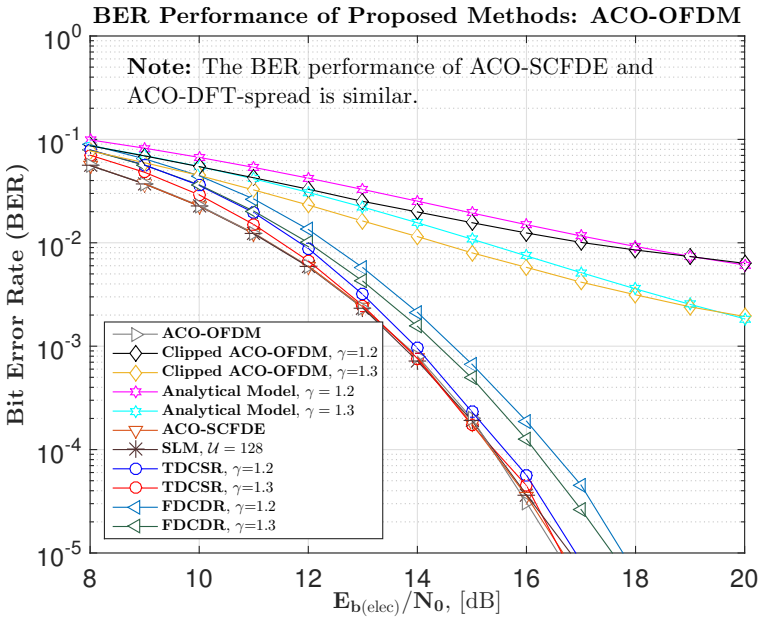

Figure 10: BER comparison of clipped ACO-OFDM, clipped ACO-OFDM with clipping mitigation using TDCSR and FDCDR, ACO-SCFDE and SLM for 16-QAM constellation and $N = 1024$. The analytical model for clipped ACO-OFDM is presented in Sec. 3.

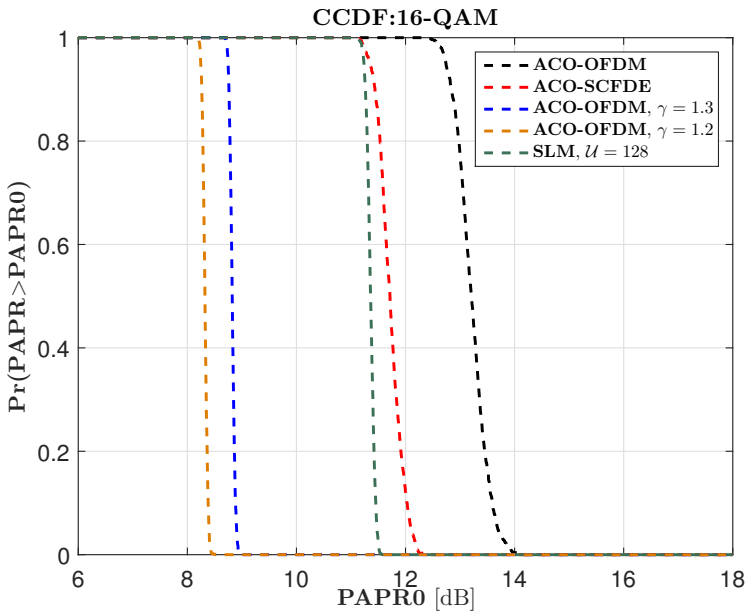

Figure 11: CCDF of PAPR comparison of clipped ACO-OFDM, ACO-OFDM, ACO-SCFDE and SLM. The clipping ratios, γ, used for clipped ACO-OFDM are 1.2 and 1.3.

6.1.2. Bit Error Rate Performance considering Quantization Noise

We assume DAC with uniform quantization and Q_b effective number of bits. A quantizer with Q_b bits defines $\mathcal{L} = 2^{Q_b}$ levels. The resolution, or step size μ, of the quantizer is the difference between two adjacent quantization levels, and is evaluated as $\mu = \triangle\xi/2^{Q_b}$, where $\triangle\xi = \xi_{\text{upper}} - \xi_{\text{lower}}$ and is equal to $\mathcal{DR}$ considered in the previous sections. Quantization noise for clipped O-OFDM can be modeled as an additive, uniformly distributed white noise, with variance given by [34]

$$\sigma^2_{\text{DAC}} = \frac{\alpha\mu^2}{12} \tag{24}$$

where α incorporates the attenuation due to signal clipping. (24) foresees that signal clipping can reduce the quantization noise. Based on the signal clipping defined in Sec. 2, the variance of quantization noise for DCO- and ACO-OFDM can be given as

$$\sigma^2_{\text{DAC}} = \begin{cases} \frac{\alpha\xi^2_{\text{upper}}}{3(2^{2Q_b})}, & \text{for DCO-OFDM} \\ \frac{\alpha\xi^2_{\text{upper}}}{12(2^{2Q_b})}, & \text{for ACO-OFDM.} \end{cases} \tag{25}$$

From (25), it can be observed that since the signal excursion of DCO-OFDM is twice the signal excursion of ACO-OFDM, the quantization noise variance for DCO-OFDM is four times greater than ACO-OFDM [34].

The BER performance of the proposed methods for DCO-OFDM by considering the joint impact

of clipping and quantization is presented in Fig. 12. The clipping ratio, γ is set equal to 1.5 for TDCSR and FDCDR, and the effective number of bits, Q_b are set equal to 5. The performance of the proposed methods is compared with SLM and conventional DCO-OFDM. Note that for DCO-OFDM and SLM, only quantization noise has been considered, and the data carrying sub-carriers have no clipping distortion. It can be observed that even in the presence of both clipping and quantization noise, the performance of TDCSR and FDCDR is superior as compared to SLM and conventional DCO-OFDM. Importantly, the result reveals that if TDCSR and FDCDR (with signal clipping) are used for DCO-OFDM, then the bit resolution of the DAC can be reduced, unlike conventional DCO-OFDM and SLM, where the high bit resolution DAC might be required.

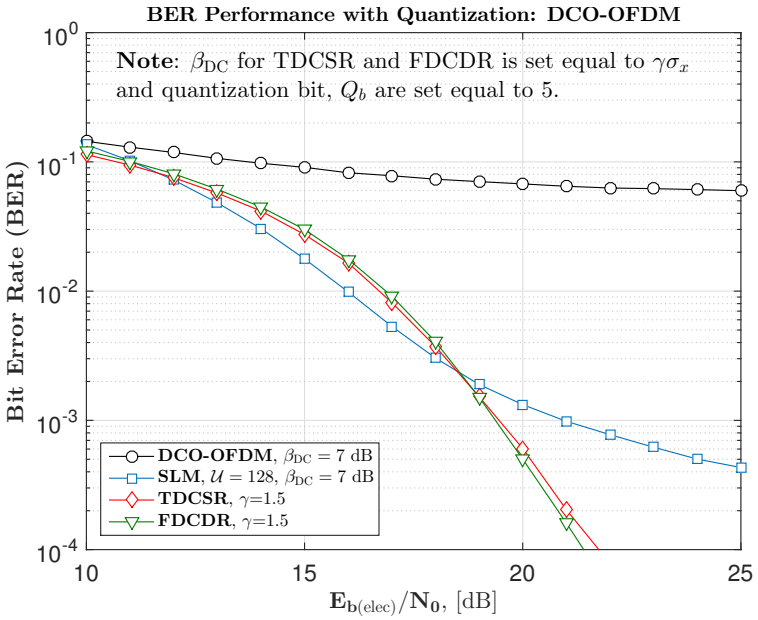

Figure 12: BER performance of TDCSR and FDCDR considering quantization noise for DCO-OFDM. The clipping ratio, γ is set equal to 1.5, the effective number of bits for quantization, Q_b are set equal to 5.

Further, the BER performance of TDCSR and FDCDR for ACO-OFDM with quantization has been presented in Fig. 13, and is compared with conventional ACO-OFDM and ACO-SCFDE (without any clipping). The quantization bits, Q_b are set equal to 3, and the clipping ratio, γ, for TDCSR and FDCDR is set equal to 1.2. It can be observed that the performance of both ACO-OFDM and ACO-SCFDE drastically degrades in the presence of strong quantization noise, whereas, the proposed methods performs efficiently in a similar scenario. Owing to (25), it can be foreseen that if the signal is clipped, the quantization noise variance, σ^2_{DAC} can be reduced, therefore, the impact of quantization on the clipped signal is less severe as compared to an unclipped signal. However, due to clipping, clipping distortion is instigated. But at the same time, the proposed methods can efficiently mitigate the clipping distortion, thus, resulting in a superior performance. It can

be concluded that for ACO-OFDM the bit resolution requirement is less compared to conventional ACO-OFDM or ACO-SCFDE if either of TDCSR and FDCDR is considered.

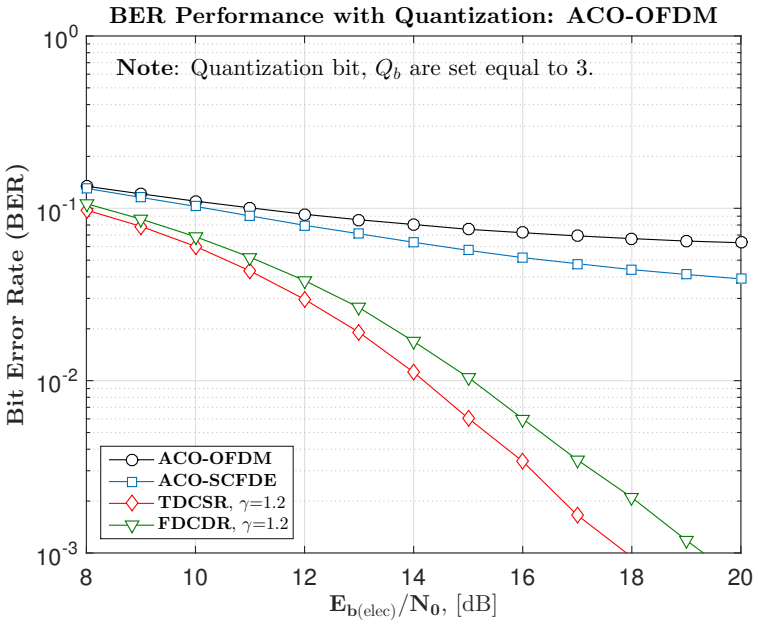

Figure 13: BER performance of TDCSR and FDCDR considering quantization noise for ACO-OFDM. The clipping ratio, γ is set equal to 1.2, the effective number of bits for quantization, Q_b are set equal to 3.

6.1.3. Bit Error Rate Performance considering Different Number of Iterations

Since both TDCSR and FDCDR are iterative, the performance evaluation with respect to the number of iterations is logical. Moreover, it can also help in understanding the tradef-off between the gain in performance and the complexity that can be tolerated for the proposed methods with each increase in an iteration. The performance of the proposed methods for DCO- and ACO-OFDM for iterations $i = 1 \rightarrow 4$ has been depicted in Fig. 14 and Fig. 15, respectively. Further, the clipping ratio, γ is set equal to 1.5 and 1.2 for DCO- and ACO-OFDM, respectively. It can be observed with each increment in iteration from $i = 1$ to $i = 3$ for the proposed methods, the performance can be significantly improved. However, the gain in performance by increasing further the number of iterations to $i = 4$ is minimal and is not worth an increase in complexity. Therefore, in simulations, three iterations are chosen for TDCSR and FDCDR. Furthermore, the complexity implications as a function of the number of iterations are presented in detail in subsequent subsection.

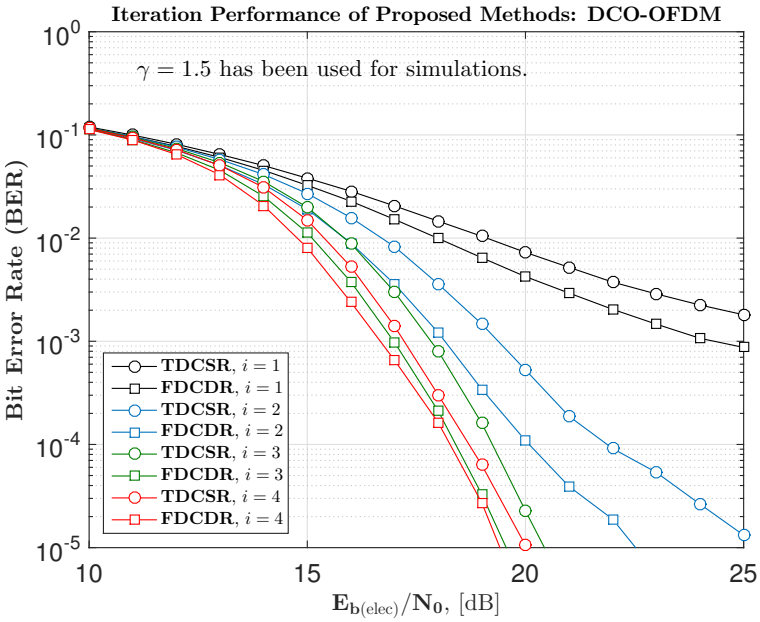

Figure 14: Performance of TDCSR and FDCDR for DCO-OFDM considering different number of iterations. The clipping ratio, γ, of 1.5 has been used for simulations.

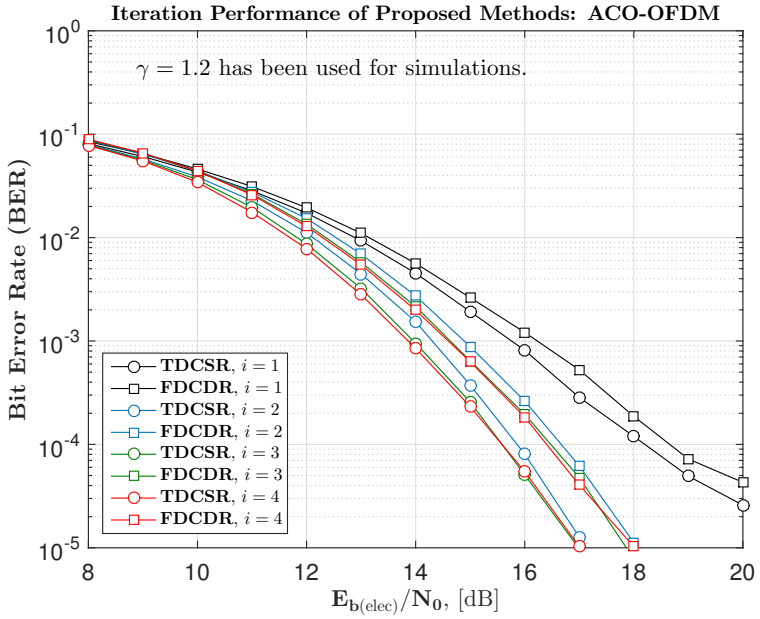

Figure 15: Performance of TDCSR and FDCDR for ACO-OFDM considering different number of iterations. The clipping ratio, γ, of 1.2 has been used for simulations.

6.1.4. Power Efficiency

Fig. 16 and Fig. 17 depict how $\langle \mathbf{E_{b(elec)}/N_0} \rangle$ (the required $\mathbf{E_{b(elec)}/N_0}$ for a BER of 10^{-3}) varies with the ratio of bit rate to the normalized bandwidth (refer to [8] and [35] for evaluation of the ratio of bit rate to normalized bandwidth) for DCO- and ACO-OFDM, respectively. Clipping ratio for 16-, 64- and 256-QAM is set equal to 1.5, 2 and 2.7, respectively for DCO-OFDM. Whereas, for ACO-OFDM, the clipping ratio is set at 1.2, 1.6 and 2.3 for 16-, 64- and 256-QAM. Clearly, both TDCSR and FDCDR achieve significant gains for DCO-OFDM, whereas, a marginal loss is observed in case of ACO-OFDM, when compared to conventional ACO-OFDM, ACO-SCFDE and SLM when no upper clipping is considered. It is important to realize that the gain for the proposed methods is significant over conventional ACO-OFDM when upper clipping is induced by the limited dynamic range of the LED, and no clipping mitigation is performed: in this case, the BER for ACO-OFDM would be above an error floor of 10^{-3} as can be seen from Fig. 10. BER degradation is also expected for ACO-SCFDE, when upper clipping is introduced. Note that the performance of TDCSR in conjunction with clipped ACO-OFDM is similar to the performance of conventional ACO-OFDM and ACO-SCFDE, but with a lower PAPR (see Fig. 11), which can be beneficial in increasing the modulation efficiency of the LED if proposed methods are used. It is worth mentioning that TDCSR suffers a 4.5 dB $\mathbf{E_{b(elec)}/N_0}$ penalty for ACO-OFDM (Fig. 17) with 256-QAM. It may come from the fact that for higher order modulations, the symbol error rate is too large to operate on a right decision, thus reconstruction of the clipped samples might no longer be efficient.

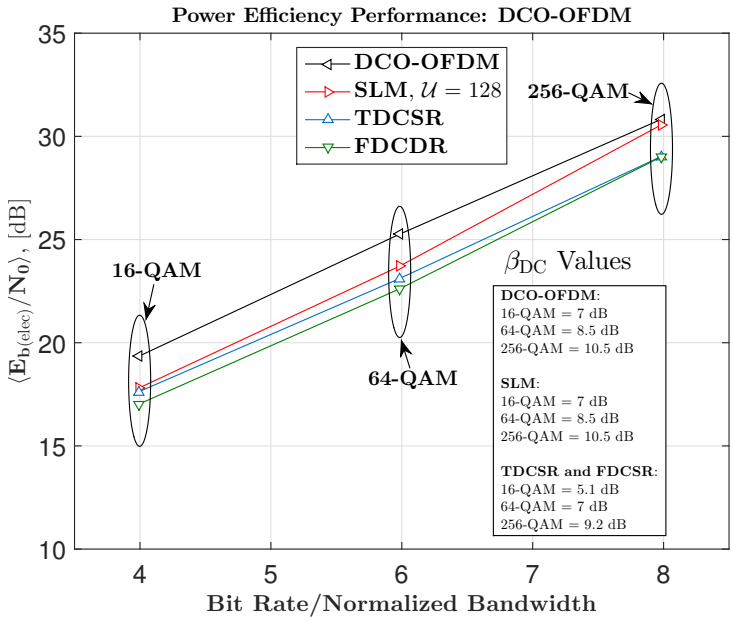

Figure 16: $\langle \mathbf{E_{b(elec)}/N_0} \rangle$ against bit rate/normalized bandwidth for DCO-OFDM, SLM, and DCO-OFDM with clipping mitigation using 16-, 64- and 256-QAM constellations and $N = 1024$. The DC bias used for each scheme is presented in the table.

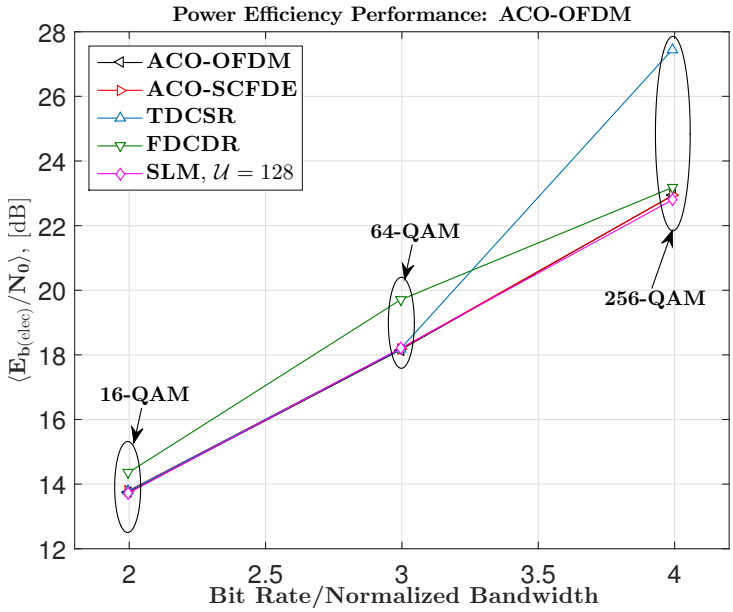

Figure 17: $\langle \mathbf{E_{b(elec)}}/\mathbf{N_0} \rangle$ against bit rate/normalized bandwidth for ACO-OFDM, ACO-SCFDE, SLM and ACO-OFDM with clipping mitigation using 16-, 64- and 256-QAM constellations and $N = 1024$.

6.2. Complexity Analysis

The complexity analysis of the proposed methods in terms of probability of convergence, theoretical runtime boundaries can be cumbersome, since the complexity of the problem is directly correlated with the size of DFT/IDFT, N. Therefore, hereby, we have evaluated the complexity of the proposed algorithm in terms of total number of operations per bit that are required as a function for DFT/IDFT size, N and constellation size, M. We consider that for O-OFDM, the IDFT and DFT operations are efficiently performed using fast Fourier transform (FFT) algorithm. N-order FFT/IFFT requires approximately $4N\log_2(N)$ real time operations, including multiplications and additions [36]. Hereafter, for simplicity we use subscript O-OFDM to take into account both DCO- and ACO-OFDM, and superscripts of $(\cdot)^{\mathrm{Tx}}$ and $(\cdot)^{\mathrm{Rx}}$ to distinguish between the transmitter and the receiver.

Only an N-order IFFT is performed at the transmitter of O-OFDM, thus, the total number of real operations required per second for the transmitter are

$$\mathcal{C}^{\mathrm{Tx}}_{\text{O-OFDM}} = \frac{4N\log_2(N)}{T_{\text{O-OFDM}}}, \tag{26}$$

with $T_{\text{O-OFDM}}$ being the transmitted O-OFDM symbol period, given as,

$$T_{\text{O-OFDM}} = NT_{\mathrm{s}}, \tag{27}$$

where T_{s} is the M-ary QAM O-OFDM symbol period, given as $T_{\mathrm{s}} = T_{\mathrm{b}}\log_2(M)$, with T_{b} being

the bit duration. Here, for simplicity, we have omitted the CP, for the reasons mentioned in Sec. 2. The overall complexity in terms of the number of real operations required per bit for O-OFDM transmitter can be given as

$$\mathcal{O}^{\text{Tx}}_{\text{O-OFDM}} = T_{\text{b}}\mathcal{C}^{\text{Tx}}_{\text{O-OFDM}} = \frac{4N\log_2(N)T_{\text{b}}}{T_{\text{O-OFDM}}} = \frac{4\log_2(N)}{\log_2(M)}. \tag{28}$$

At the receiver, complex single-tap equalization on each used sub-carriers, N_u, has to be taken into account. Since, Hermitian symmetry is enforced on the frequency-domain data-symbol vector, and the zeroth and $N/2$th sub-carriers are set equal to zero to avoid any DC shift, the used sub-carriers, N_u for DCO- and ACO-OFDM will be equal to $N/2-1$ and $N/4$, respectively. Considering an N-order FFT at the receiver, and that the complex multiplications (for equalization) are implemented using four real multiplications two real additions [36], then, the number of real operations required per second for O-OFDM receiver can be given as

$$\mathcal{C}^{\text{Rx}}_{\text{O-OFDM}} = \frac{[4N\log_2(N)+6N_u]}{T_{\text{O-OFDM}}}. \tag{29}$$

Taking into account (29), the complexity of O-OFDM receiver in terms of number of real operations per bit can be evaluated as

$$\mathcal{O}^{\text{Rx}}_{\text{O-OFDM}} = T_{\text{b}}\mathcal{C}^{\text{Rx}}_{\text{O-OFDM}} = \frac{[4N\log_2(N)+6N_u]\,T_{\text{b}}}{T_{\text{O-OFDM}}} = \frac{4N\log_2(N)+6N_u}{N\log_2(M)}. \tag{30}$$

Combining (26), (27) and (29), the overall complexity order of O-OFDM (for both transmitter and receiver) in terms of the number of real operations per bit can be given as

$$\mathcal{O}^{\text{Tx+Rx}}_{\text{O-OFDM}} = \frac{8N\log_2(N)+6N_u}{N\log_2(M)}. \tag{31}$$

Observe that the complexity of both DCO- and ACO-OFDM can be evaluated using (31), by changing, the number of used sub-carriers, N_u.

We now move on to accessing the complexity of proposed methods. For TDCSR, the transmitter complexity will be exactly the same as that for O-OFDM, since no additional real time operations per bit are required. However, at the receiver employing TDCSR, apart from the standard N-order FFT and equalization, additional N-order FFT and IFFT per iteration and an N-order IFFT (step (01) of TDCSR) are required. Thus, the number of real operations per bit for receiver employing TDCSR is given as

$$\mathcal{O}^{\text{Rx}}_{\text{TDCSR}} = \frac{(i+1)8N\log_2(N)+6N_u}{N\log_2(M)} \tag{32}$$

and the overall complexity of the transmitter and the receiver in terms of the number of real operations per bit is

$$\mathcal{O}^{\text{Tx+Rx}}_{\text{TDCSR}} = \frac{(i+1.5)8N\log_2(N)+6N_u}{N\log_2(M)}. \tag{33}$$

(33) can also be used for both DCO- and ACO-OFDM with different N_u. For FDCDR, similar to TDCSR and O-OFDM, the transmitter complexity of the system employing FDCDR will be equal to the conventional O-OFDM. However, at the receiver, N-order FFT and IFFT per iteration are needed in addition to standard N-order FFT and equalization. Therefore, the total number of real operations per bit for receiver employing FDCDR is given as

$$\mathcal{O}_{\text{FDCDR}}^{\text{Rx}} = \frac{(2i+1)4N\log_2(N) + 6N_u}{N\log_2(M)}. \tag{34}$$

From (34), the complexity of O-OFDM with FDCDR in terms of the number of real operations per bit is evaluated as

$$\mathcal{O}_{\text{FDCDR}}^{\text{Tx+Rx}} = \frac{(i+1)8N\log_2(N) + 6N_u}{N\log_2(M)}. \tag{35}$$

Observe that TDCSR is marginally more complex as compared to FDCDR because of the presence of an additional N-order IFFT which is used only once for the method.

As in simulation results, we have compared the performance of proposed clipping mitigation methods with that of SLM and ACO-SCFDE, therefore, here we also evaluate the complexity implication of both SLM and ACO-SCFDE. For SLM, the additional complexity is at both transmitter and at the receiver, compared to O-OFDM. At the transmitter for O-OFDM using SLM, the N-order IFFT required is correlated to number of phase vectors, $\mathcal{U}$, that have been used. Thus, the complexity of O-OFDM transmitter with SLM in terms of real time operations per bit is given as

$$\mathcal{O}_{\text{SLM}}^{\text{Tx}} = \frac{4\mathcal{U}\log_2(N)}{\log_2(M)}. \tag{36}$$

Moreover, at the receiver, apart from standard N-order FFT and equalization, N multiplications are required to recover the original data block that has been transmitted. Consequently, the complexity in terms of real time operations per bit for O-OFDM receiver employing SLM can be given as

$$\mathcal{O}_{\text{SLM}}^{\text{Rx}} = \frac{4N\log_2(N) + N + 6N_u}{N\log_2(M)}. \tag{37}$$

Combining (36) and (37), the overall complexity in terms of the number of real operations required per bit for O-OFDM employing SLM can be given as

$$\mathcal{O}_{\text{SLM}}^{\text{Tx+Rx}} = \frac{(\mathcal{U}+1)4N\log_2(N) + N + 6N_u}{N\log_2(M)}. \tag{38}$$

As discussed in simulation results, a large number of phase vectors, $\mathcal{U}$ are required for SLM to significantly counteract the high PAPR, thus drastically increase the complexity. By performing simulations under different clipping scenarios, we have observed that three iterations of the iterative algorithms are enough to mitigate the clipping noise. As a result, if we compare the complexity of TDCSR and FDCDR with SLM using (33) , (35) and (38) considering $i = 3$ and $\mathcal{U} = 128$ (128 phase vectors are used since we have already established that a large number of phase vectors

are required to significantly mitigate PAPR), we can conclude that the complexity of SLM is exponentially greater than both TDCSR and FDCDR.

Further, considering ACO-SCFDE, the block diagram of which is depicted in Fig. 3, it can be observed that additional $N/4$-order IFFT and FFT are required at the transmitter and receiver, respectively. So, the complexity in terms of the number of real operations required per bit for ACO-SCFDE at the transmitter and receiver is given by

$$\mathcal{O}^{\text{Tx}}_{\text{ACO-SCFDE}} = \frac{5N\log_2(N) - 2N}{N\log_2(M)} \tag{39}$$

and

$$\mathcal{O}^{\text{Rx}}_{\text{ACO-SCFDE}} = \frac{5N\log_2(N) - 2N + 6N_u}{N\log_2(M)}, \tag{40}$$

respectively. The overall complexity order in real operations per bit for ACO-SCFDE implementation can be obtained by combining (39) and (40) as

$$\mathcal{O}^{\text{Tx+Rx}}_{\text{ACO-SCFDE}} = \frac{10N\log_2(N) - 4N + 6N_u}{N\log_2(M)}. \tag{41}$$

Comparing (31) and (41), we observe that ACO-SCFDE is slightly more complex as compared to conventional ACO-OFDM, however, comparing (33) and (35) with (41), it can be observed that ACO-SCFDE is less complex as compared to ACO-OFDM employing either TDCSR or FDCDR. However, if ACO-OFDM with TDCSR or FDCDR is used, a drastic PAPR reduction can be achieved (Fig. 11). Moreover, the quantization noise is also less due to reduced signal range as a result of clipping, as discussed previously in simulation results.

7. Conclusion

In this work, deliberate clipping has been adopted to limit the high peaks of O-OFDM signal to pre-defined threshold. Two decision-directed iterative methods are proposed to mitigate the distortions instigated because of signal clipping. From this study, we conclude the following:

1. The proposed methods can efficiently mitigate clipping distortion for both DCO- and ACO-OFDM.
2. TDCSR and FDCDR achieve significant performance gain over conventional DCO-OFDM when used for DCO-OFDM, whereas, there exits a marginal performance loss for ACO-OFDM over conventional ACO-OFDM and ACO-SCFDE. However, it is important to realize that if clipping is introduced by the LED, a drastic degradation in performance for conventional ACO-OFDM and ACO-SCFDE is expected.
3. The PAPR reduction due to clipping of DCO-OFDM is greater compared to SLM, since the PAPR reducing capability of SLM using different phase vectors is inherently less efficient. Furthermore, the BER achieved by employing either TDCSR or FDCDR for DCO-OFDM is better compared to SLM.

4. TDCSR and FDCDR exhibit comparable BER performance as that of ACO-OFDM, ACO-SCFDE and SLM, however, peak power reduction due to clipping is considerably high, whereas, the reduction in peak power using ACO-SCFDE and SLM is less. Moreover, the clipped ACO-OFDM can have an improved modulation power as compared to ACO-OFDM/ACO-SCFDE.
5. The linear range of clipped O-OFDM is less compared to conventional O-OFDM and SCFDE techniques, resulting is a pronounced reduction in quantization noise. Thus facilitating the practical implementation of O-OFDM with limited bit resolution DACs.
6. FDCDR performs better for DCO-OFDM compared to TDCSR. Whereas, TDCSR has better performance for ACO-OFDM for low order constellations, i.e., 16- and 64-QAM.
7. The total number of real operations per bit required for FDCDR in conjunction with O-OFDM are less compared to when TDCSR is used.
8. The overall complexity of TDCSR and FDCDR is less compared to SLM, since a large number of phase vectors are required to significantly reduce the PAPR. Whereas, less iterations of TDCSR and FDCDR are needed. Moreover, the number of operations for TDCSR and FDCDR are high compared to ACO-SCFDE, however, for complexity analysis, the overall complexity of the system should be considered, which also includes the complexity of the DAC. For ACO-SCFDE, the DAC has a large bit resolution requirement, however, when either TDCSR or FDCDR with clipping is used with O-OFDM, the bit resolution can be relaxed.

It is concluded that with a moderate number of iterations and additional complexity, the presented methods can be of interest for PAPR reduction in IM-DD O-OFDM systems.

References

[1] Carruthers J. B. and J. M. Kahn. Multiple-subcarrier modulation for nondirected wireless infrared communication. *IEEE J. Sel. Areas Commun.*, 14(3):538–546, 1996.

[2] W. O. Popoola, Z. Ghassemlooy, and B. G. Stewart. Pilot-assisted PAPR reduction technique for optical OFDM communication systems. *J. of Lightw. Tech.*, 32(7):1374–1382, 2014.

[3] Z. Yu, R. J. Baxley, and G. T. Zhou. EVM and achievable data rate analysis of clipped OFDM signals in visible light communication. *EURASIP J. Wireless Commun. Network.*, 2012(1):1–16, 2012.

[4] R. Narasimhan and M. D. Audeh. Effect of electronic-ballast fluorescent lighting on wireless infrared links. *IEE Proc. Optoelectron.*, 143(6):347–354, 1996.

[5] S. Dimitrov, S. Sinanovic, and H. Hass. Clipping noise in OFDM-based optical wireless communication systems. *IEEE Trans. Commun.*, 60(4):1072–1081, 2012.

[6] D. J. F. Barros, S. K. Wilson, and J. M. Kahn. Comparison of orthogonal frequency-division multiplexing and pulse-amplitude in indoor optical wireless links. *IEEE Trans. Commun.*, 60(1):153–163, 2012.

[7] J. Armstrong and A. J. Lower. Power efficient optical OFDM. *Electron. Lett*, 42(6):370–372, 2006.

[8] J. Armstrong and B. J. C. Schmidt. Comparison of asymmetrically clipped optical OFDM and DC-biased optical OFDM in AWGN. *IEEE Commun. Lett.*, 12(5):343–345, 2008.

[9] C. R. Berger, Y. Benlachtar, R. I. Killey, and P. A. Milder. Theoretical and experimental evaluation of clipping and quantization noise for optical OFDM. *Opt. Express*, 19(18):17713–17728, 2011.

[10] L. Nadal, M. S. Moreolo, J. M. Fabrega, and G. Junyent. Comparison of peak power reduction techniques in optical OFDM systems based on FFT and FHT. *Intl. Conf. on Transparent Opt. Networks*, pages 1–4, 2011.

[11] R. You and J. M. Kahn. Average power reduction techniques for multiple-subcarrier intensity-modulated optical signals. *IEEE Trans. Commun.*, 49(12):2164–2171, 2001.

[12] W. Kang and S. Hranilovic. Power reduction techniques for multiple-subcarrier modulated diffuse wireless optical channels. *IEEE Trans. Commun.*, 56(2):279–288, 2008.

[13] K. Acolatse, Y. Bar-Ness, and S. K. Wilson. Novel techniques of single-carrier frequency-domain equalization for optical wireless communications. *EURASIP J. Adv. Sig. Process.*, 2011:4, 2011.

[14] J. Zhou, Z. Zhang, T. Zhang, M. Guo, X. Tang, Z. Wang, , and Y. Qiao. A combined PAPR-reduction technique for asymmetrically clipped optical OFDM system. *Opt. Commun.*, pages 451–456, 2016.

[15] Z. Fulai, L. Luokun, and Y. Jinjin. DFT-spread combined with PTS method to reduce the PAPR in VLC-OFDM system. *Intl. Conf. on Soft. Engineer. Ser. Sci.*, pages 629–632, 2014.

[16] C. Wu, H. Zhang, and W. Xu. On visible light communication using LED array with DFT-spread OFDM. *IEEE ICC*, pages 3325–3330, 2014.

[17] J. Zhou and Y. Qiao. Low-PAPR asymmetrically clipped optical OFDM for intensity-modulation/direct-detection systems. *IEEE Photon. J.*, 7(3):1–8, 2015.

[18] J. Zhou and Y. Qiao. Low-peak-to-average power ratio and low-complexity asymmetrically clipped optical orthogonal frequency-division multiplexing uplink transmission scheme for long-reach passive optical network. *Optics letters*, 40(17):4034–4037, 2015.

[19] H. Zhang, Y. Yuan, and W. Xu. PAPR reduction for DCO-OFDM visible light communications via semidefinite relaxation. *IEEE Photon. Technol. Lett.*, 26(17):1718–1721, 2014.

[20] W. Xu, M. Wu, H. Zhang, X. You, and C. Zhao. ACO-OFDM-specified recoverable upper clipping with efficient detection for optical wireless communications. *IEEE Photon. J.*, 6(5):1–17, 2014.

[21] A. Ali, A. Al-Rabah, M. Masood, and T. Y. Al-Naffouri. Receiver-based recovery of clipped OFDM sig. for PAPR reduction: A Bayesian approach. *IEEE Access*, 2:1213–1224, 2014.

[22] Ali W. Azim, Y. Le Guennec, and G. Maury. Enhanced DC-biased optical OFDM for intensity-modulated optical OFDM access systems. *Intl. Conf. on Transparent Opt. Networks*, pages 1–4, 2016.

[23] Ali W. Azim, Y. Le Guennec, and G. Maury. OFDM for optical wireless systems under severe clipping conditions. *IEEE Intl. Conf. Advances in Wireless and Optical Commun.*, pages 1–4, 2016.

[24] D. Kim and G. L. Stüber. Clipping noise mitigation for OFDM by decision-aided reconstruction. *IEEE Commun. Lett.*, 3(1):4–6, 1999.

[25] J. Tellado, L. M. C. Hoo, and J. M. Cioffi. Maximum-likelihood detection of nonlinearly distorted multicarrier symbols by iterative decoding. *IEEE Trans. Commun.*, 51(2):218–228, 2003.

[26] D. Tsonev, S. Sinanovic, and H. Haas. Enhanced subcarrier index modulation (SIM) OFDM. *IEEE GLOBECOM*, pages 728–732, 2011.

[27] S. H. Han and J. H. Lee. An overview of peak-to-average power ratio reduction techniques for multicarrier transmission. *IEEE Wireless Commun.*, 12(2):56–65, 2005.

[28] J. Armstrong. OFDM for optical communications. *J. Lightw. Tech.*, 27(3):189–204, 2009.

[29] H. Elgala, R. Mesleh, and H. Haas. Practical considerations for indoor wireless optical system implementation using ofdm. *IEEE ConTEL*, pages 25–29, 2009.

[30] A. Weiss, A. Yeredor, and M. Shtaif. Iterative symbol recovery for power-efficient dc-biased optical ofdm systems. *J. Lightw. Techn.*, 34(9):2331–2338, 2016.

[31] H. Elgala, R. Mesleh, and H. Haas. Non-linearity effects and predistortion in optical ofdm wireless transmission using leds. *Intl. J. of Ultra Wideband Commun. Syst.*, 1(2):143–150, 2009.

[32] H. Ochiai and H. Imai. Performance analysis of deliberately clipped OFDM signals. *IEEE Trans. Commun.*, 50(1):89–101, 2002.

[33] J. J. Bussgang. Crosscorrelation functions of amplitude-distorted gaussian signals. *Res. Lab. Electron, Masssachusetts Inst. Tech., Cambridge, MA, USA, Tech. Rep*, 1952.

[34] J. K. Perin, M. Sharif, and J. M. Kahn. Modulation schemes for single-laser 100 Gb/s links: Multicarrier. *J. Lightw. Techn.*, 33(24):5122–5132, 2015.

[35] S. D. Dissanayake and J. Armstrong. Comparison of ACO-OFDM, DCO-OFDM and ADO-OFDM in IM/DD systems. *J. Lightw. Techn.*, 31(7):1063–1072, 2013.

[36] S. G. Johnson and M. Frigo. A modified split-radix FFT with fewer arithmetic operations. *IEEE Trans. Sig. Process.*, 55(1):111–119, 2007.